Iran J Sci Technol Trans Civ Eng (2019) 43:297–325
https://doi.org/10.1007/s40996-018-0142-z

RESEARCH PAPER

Performance Evaluation of Gravity Dams Subjected to Near- and Far-Fault Ground Motion Using Euler Approaches

A. C. Altunisik[1] · H. Sesli[1] · M. Hüsem[1] · M. Akköse[1]

Received: 1 February 2016 / Accepted: 25 July 2018 / Published online: 1 August 2018

Abstract
Ground motions in near source region of large crustal earthquakes are significantly affected by rupture directivity and tectonic fling. These effects are the strongest at longer periods, and they can have a significant impact on engineering structure. This paper focuses on the effects of long-period pulse of near-fault ground motions on the structural performance of concrete gravity dams. Three sets of near- and far-fault ground motion records, which have approximately the same peak ground acceleration, are selected from 1987 Superstitn Hills (B), 1989 Loma Prieta and 1994 Northridge earthquakes. As a case study, Sarıyar concrete gravity dam located on the Sakarya River, which is 120 km to the northeast of Ankara, is selected to investigate the near-fault ground motion effects on dam responses. The finite element models of the dam are constituted considering dam-reservoir-foundation interaction using ANSYS software. The behavior of reservoir is taken into account by using Euler approach. To determine the structural response of the dam, the linear transient analyses are performed using above-mentioned ground motion records. In the analyses, element matrices are computed using the Gauss numerical integration technique. The Newmark method is used in the solution of the equation of motions. Rayleigh damping is considered. At the end of the analyses, dynamic characteristics, maximum displacements, maximum and minimum principal stresses and maximum and minimum principal strains are attained and compared with values obtained from analyses under far-fault ground motions recorded far away from the same sites at above-mentioned earthquakes with approximately same peak ground acceleration.

Keywords Concrete gravity dam · Dam–reservoir–foundation interaction · Euler approach · Far fault · Near fault

1 Introduction

Dams are huge structures which have contributed to the development of civilization for a long time. Dams have classified in several categories as regards size, construction purpose and type. Concrete gravity dams are a type of dam built in order to meet the increasing demands for power, irrigation and drinking water, etc. They are built in many areas with active seismic activities and store a large amount of water, but failures of them cause irreparable loss of life. Therefore, during design, accuracy of assumptions and seismic safety evaluations forms the main stage for safety and operating time.

Earthquake is one of the most important dynamic problems for stability and safety of concrete gravity dams during operation. Strong ground motions due to earthquakes are significantly different nearby a fault than at a distance far away from it. So, seismic excitations can be called as near-fault and far-fault earthquakes. The differences can be observed with period and maximum velocity pulse amplitude. Especially, the velocity pulse is specific characteristics for near-fault ground motion records that cannot be seen in far-fault records (Yahyai et al. 2011).

Near-fault ground motions, recorded in recent earthquakes (1989 Loma Prieta, 1994 Northridge, 1995 Japan

✉ A. C. Altunisik
ahmetcan8284@hotmail.com

H. Sesli
hasan_sesli@hotmail.com

M. Hüsem
mhusem@ktu.edu.tr

M. Akköse
akkose@ktu.edu.tr

[1] Department of Civil Engineering, Karadeniz Technical University, Trabzon, Turkey

Table 1 Properties of selected near-fault and far-fault ground motion records. (Reproduced with permission from PEER 2013)

Ground motion	Earthquake	Component	PGA (m/s^2) g	PGV (cm/s)	PGV/PGA (s)	Mw	Distance to fault (km)
Near fault	1987 superstition hills (B)	PTS225	0.45	112.0	0.25	6.7	0.7
Far fault	1987 Superstition Hills (B)	POE270	0.45	35.7	0.08	6.7	12.4
Near fault	1989 Loma Prieta	CLS090	0.48	45.2	0.10	7.1	5.1
Far fault	1989 Loma Prieta	CYC285	0.48	39.7	0.08	7.1	21.8
Near fault	1994 Northridge	RR318	0.47	73.0	0.16	6.7	7.1
Far fault	1994 Northridge	STN20	0.47	34.6	0.08	6.7	30.0

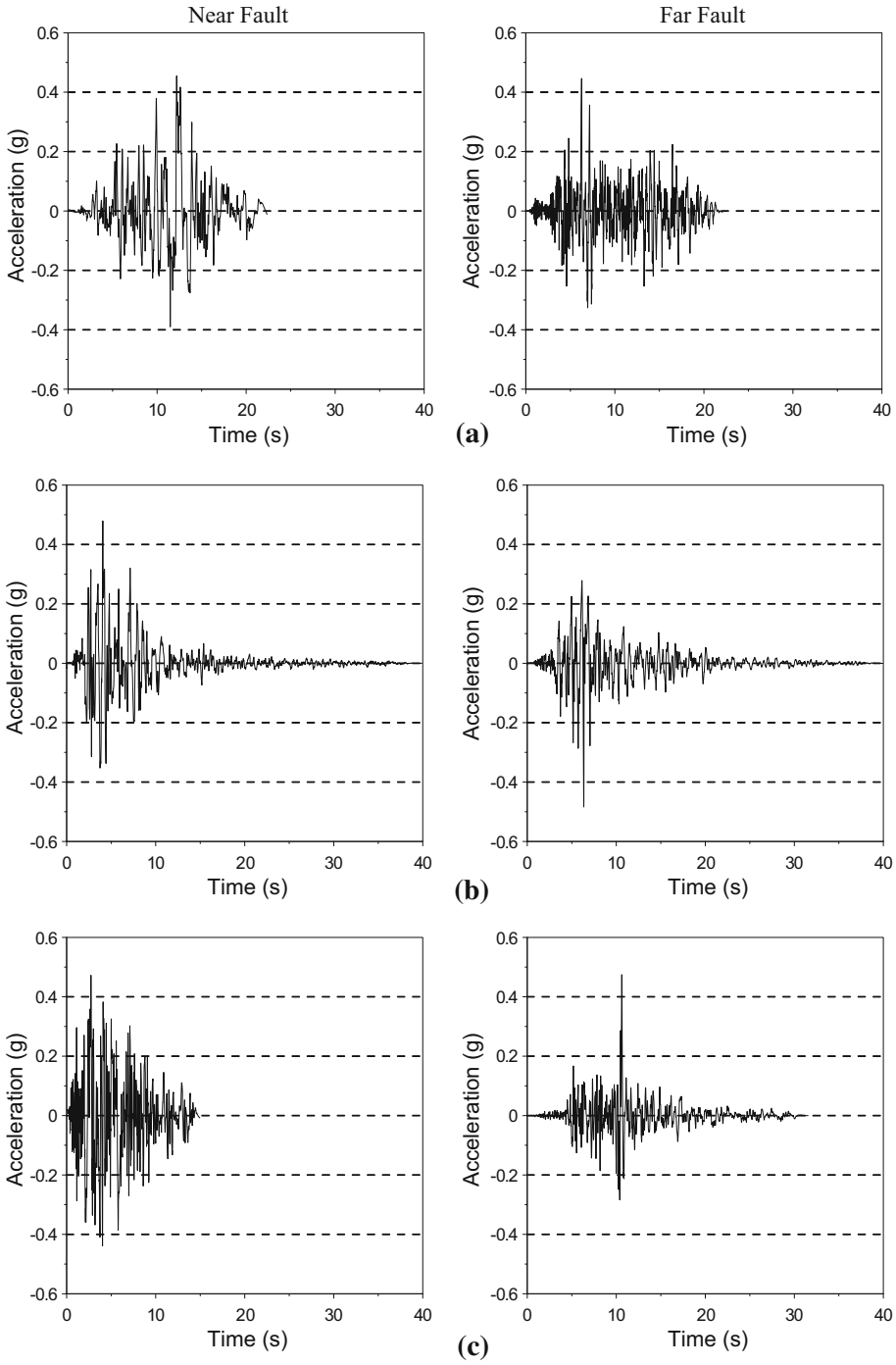

Fig. 1 Acceleration time histories of near- and far-fault ground motions obtained from **a** 1987 Superstition Hills (B), **b** 1989 Loma Prieta and **c** 1994 Northridge earthquakes

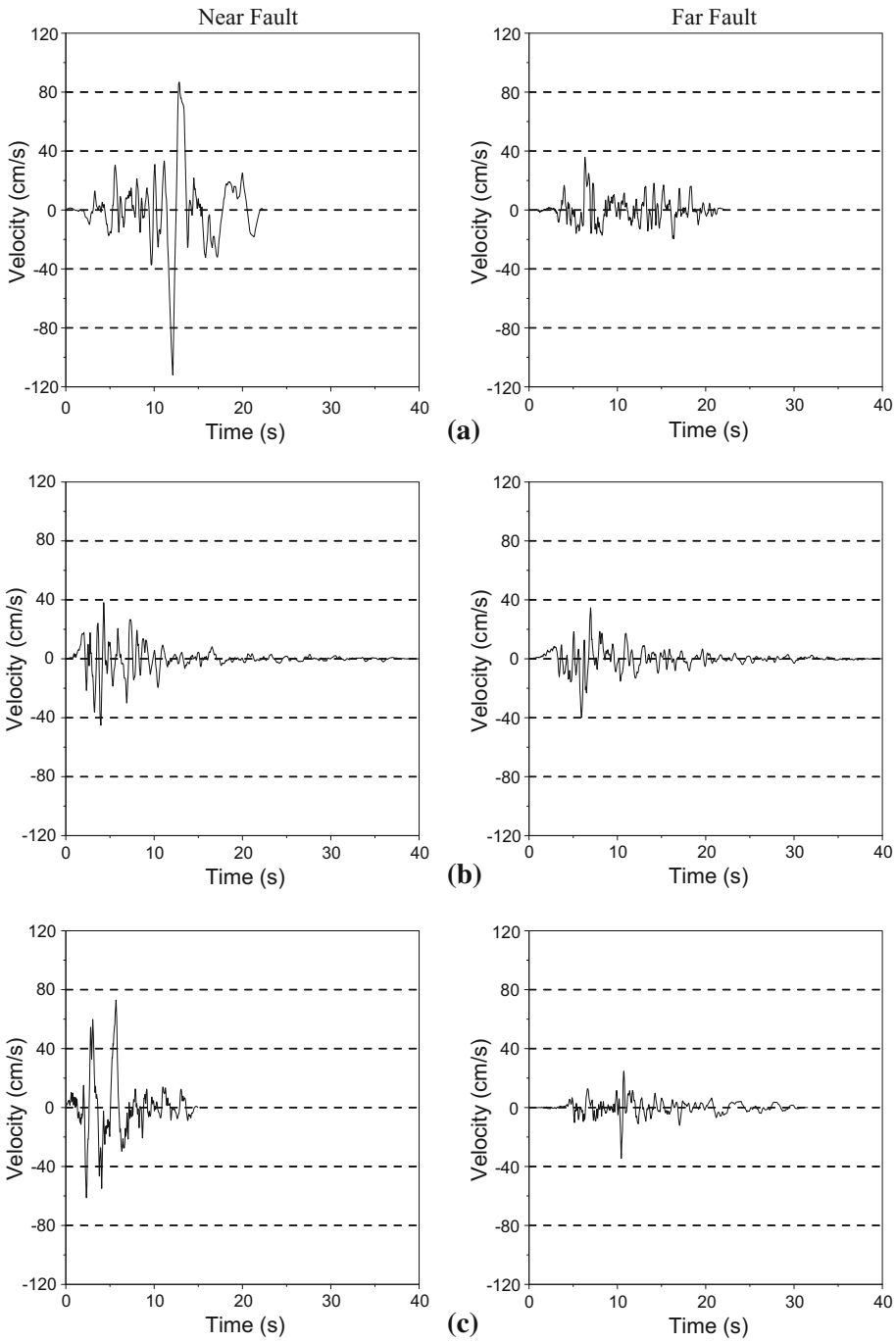

Fig. 2 Velocity time histories of near- and far-fault ground motions obtained from **a** 1987 Superstition Hills (B), **b** 1989 Loma Prieta and **c** 1994 Northridge earthquakes

Hyogoken-Nanbu, 1999 Taiwan Chi–Chi), are characterized by a ground motion with large velocity pulse which expose the structure to high input energy in the beginning of the earthquake. Because of unique/damaging characteristics of near-fault ground motion, determination of the seismic response of civil engineering structures (buildings, tunnels, bridges, nuclear stations, towers, viaducts wind turbine, tanks, etc.) in design and restoration phases using near-fault ground motion has received a great deal of attention over the last decades.

Some papers can be obtained in the literature about the static and dynamic behavior of engineering structures using near- and far-fault ground motion records. Hall et al. (1995) studied about near source ground motion effect on flexible buildings. Alavi and Krawinkler (2000) investigated the inelastic response of buildings subject to pulse type motions with the objective of incorporating the special response features in the design process. MacRae and Mattheis (2000) assessed the seismic behavior of a three-story steel framed building using three-dimensional

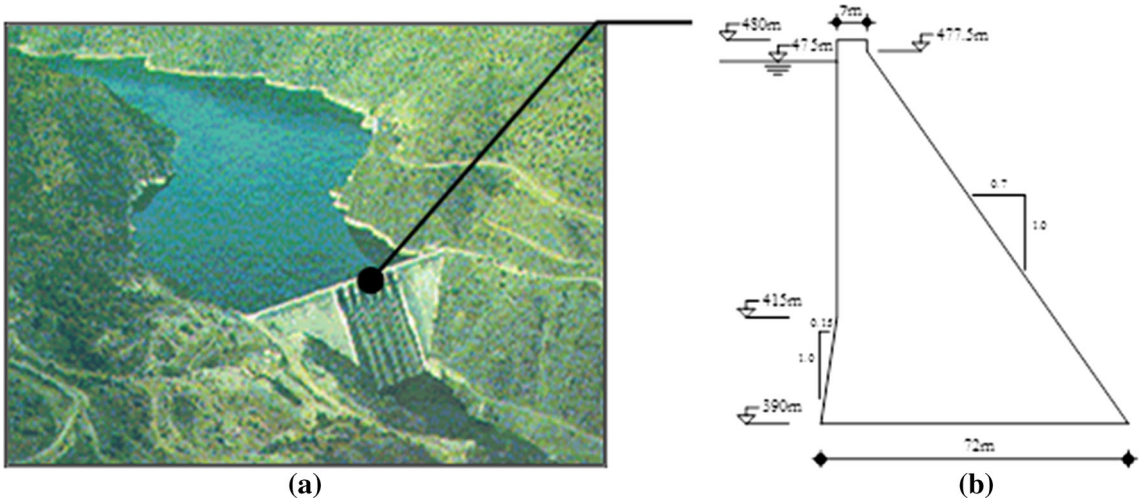

Fig. 3 Sarıyar concrete gravity dam. (Reproduced with permission from Altunisik and Sesli 2015)

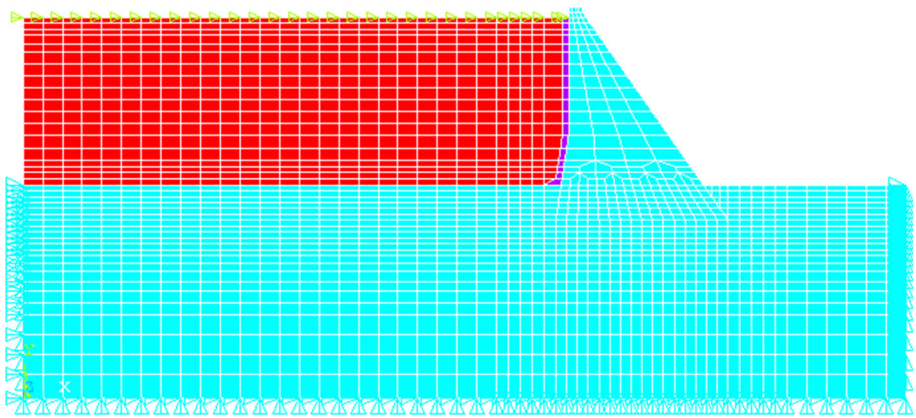

Fig. 4 Two-dimensional finite element model of Sarıyar concrete gravity dam including dam-reservoir-foundation systems using Euler approach

Table 2 Material properties used in the analyses

Material	Material properties		
	Modulus of elasticity (N/m)	Poisson's ratio (−)	Mass per unit Vol. (kg/m^3)
Dam (concrete)	35.0E9	0.15	2400
Foundation	30.0E9	0.20	–
Reservoir	20.7E8	–	1000

dynamic inelastic time history analyses under near-fault as well as code design level earthquake records. Chopra and Chintanapakdee (2001) compared the response of SDF systems under near- and far-fault earthquake motions in the context of spectral regions. Alavi and Krawinkler (2004) studied about the strengthening of moment-resisting frame structures against near-fault ground motion effects. Liao et al. (2004) compared dynamic response of isolated and non-isolated continuous girder bridges subjected to near-fault ground motions. Park et al. (2004) performed simulation of seismic performance of the Bolu Viaduct subjected to near-fault ground motions. Shen et al. (2004) investigated a seismically isolated bridge under near-fault earthquake ground motions. Yan and Lee (2007) examined traveling wave effect on the seismic response of a steel arch bridge subjected to near-fault ground motions.

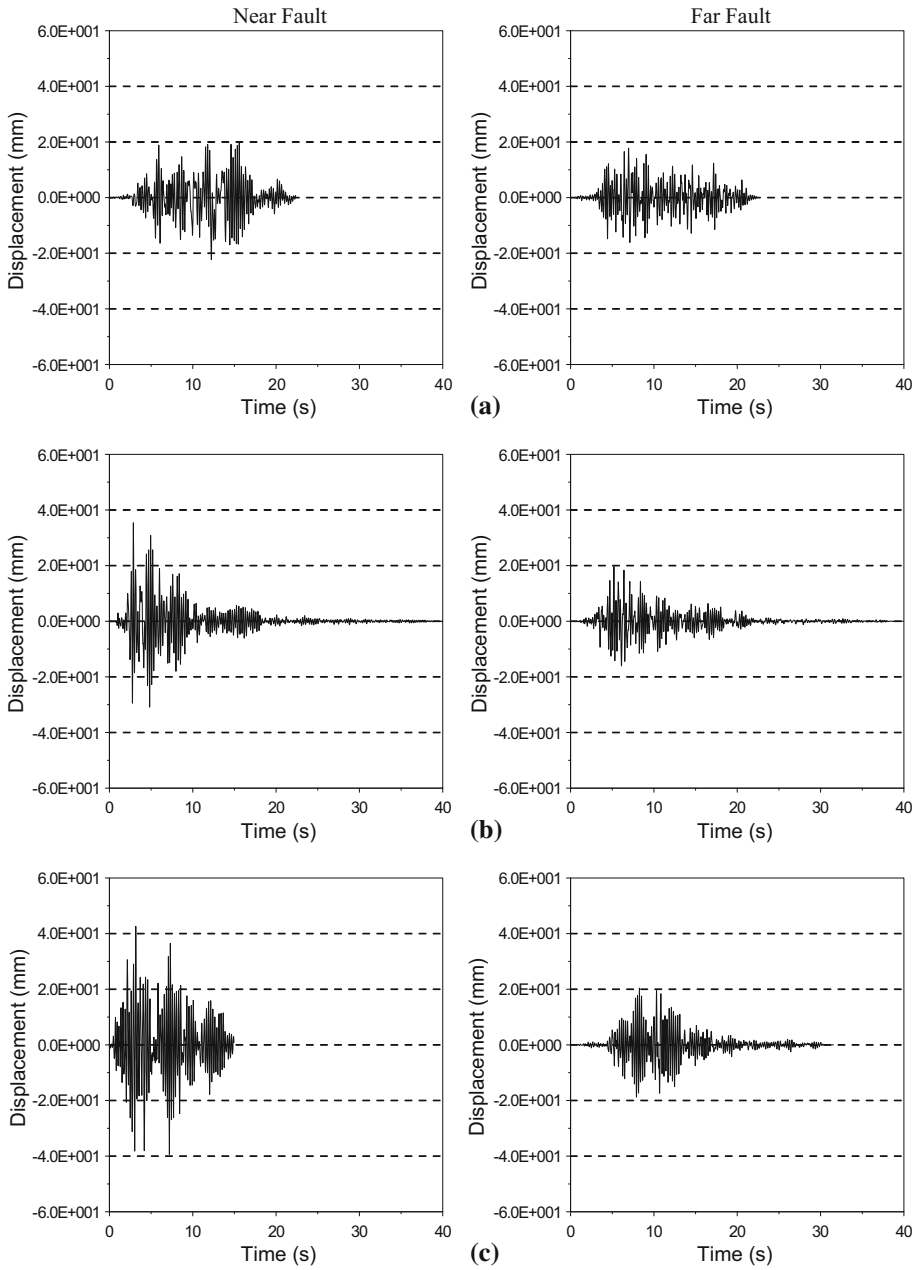

Fig. 5 Time histories of horizontal displacements at the crest point for **a** 1987 Superstition Hills (B), **b** 1989 Loma Prieta and **c** 1994 Northridge earthquakes

Providakis (2007) carried out pushover analysis of base-isolated steel concrete composite structures under near-fault excitations. Phan et al. (2007) investigated near-fault ground motion effects on reinforced concrete bridge columns. Su et al. (2007) presented analytical investigations of seismic responses for reinforced concrete bridge columns subjected to strong near-fault ground motions. Bayraktar et al. (2009) compared near- and far-fault ground motion effect on the nonlinear response of dam–reservoir–foundation systems. Akköse and Şimşek (2010) investigated nonlinear seismic response of concrete gravity dams to near-fault ground motions including dam–water–sediment–foundation interactions. Jonsson et al. (2010) presented earthquake response of a base-isolated bridge subjected to strong near-fault ground motion. Corigliano and Scandella (2011) studied on seismic analysis of deep

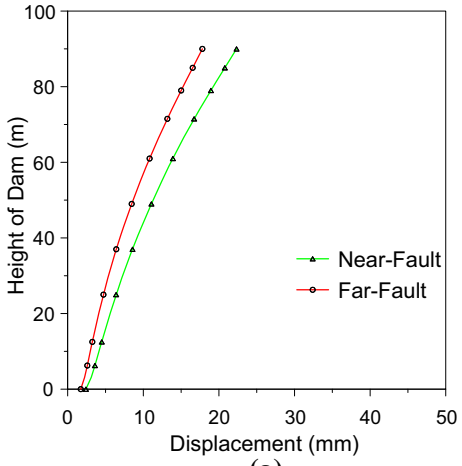

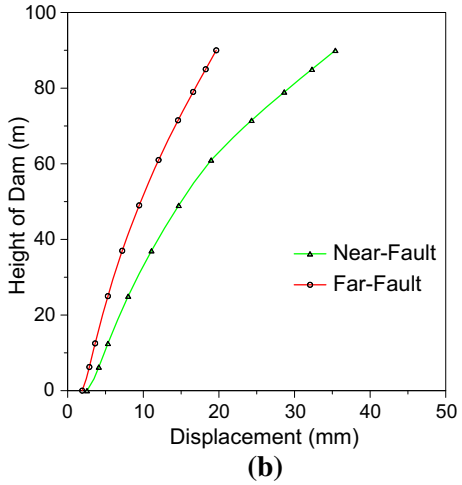

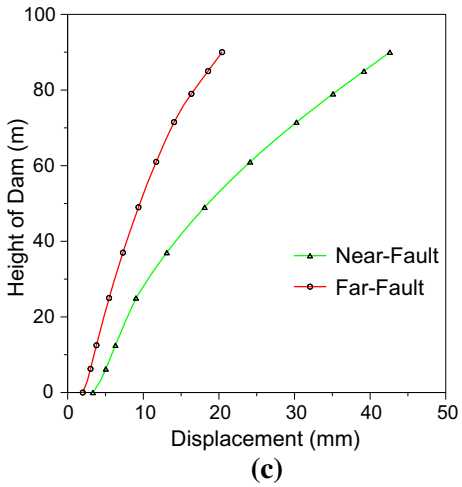

Fig. 6 Maximum horizontal displacements by height of Sarıyar concrete gravity dam for **a** 1987 Superstition Hills (B), **b** 1989 Loma Prieta and **c** 1994 Northridge earthquakes

tunnels in near-fault conditions in southern Italy. Yahyai et al. (2011) investigated effect of near-fault earthquakes with forward directivity on telecommunication towers. Karalar et al. (2012) realized parametric analysis of optimum isolator properties for bridges susceptible to near-fault ground motions. Adanur et al. (2012) presented a comparison of near-fault and far-fault ground motion effects on geometrically nonlinear earthquake behavior of suspension bridges. Stamatopoulos (2012) investigated response of a wind turbine subjected to near-fault excitation. Zhang and Wang (2013) investigated effects of near-fault and far-fault ground motions on nonlinear dynamic response and seismic damage of concrete gravity dams. Amiri et al. (2013) estimated seismic demands of steel frames subjected to near-fault earthquakes having forward directivity and compared them with pushover analysis results. Panchal and Jangid (2014) aimed to investigate the behavior of liquid storage tanks with variable curvature friction pendulum system (VCFPS) under near-fault ground motions. Gang et al. (2014) showed the effect of tower-line coupling on seismic responses of large crossing transmission tower-line system subject to far field ground motions. Antonellis and Panagiotou (2014) evaluated the seismic response of bridges with rocking foundations compared to fixed-base bridges at near-fault site. Ghaffarzadeh et al. (2015) performed a numerical study to evaluate the near-fault ground motions effect on a building equipped with friction damping system with amplifying braces. Huang (2015) examined the nonlinear dynamic behavior of gravity dams under several near-fault earthquakes. Tzimas et al. (2016) evaluated the potential of post-tensioned self-centering moment-resisting frames and viscous dampers to reduce the collapse risk and improve the residual drift performance of steel buildings in near-fault regions. Ismail et al. (2016) presented roll-in-cage isolator as an alternative isolation bearing for efficient protection of common highway bridge structures. Beiraghi et al. (2016) investigated the different energy demands for the 20-story, 30-story and 40-story tall core wall buildings with 1PH (plastic hinge), 2PH, 3PH and WPH approaches over the structure height under the far-fault and near-fault earthquakes. Yazdani and Alembagheri (2017) studied on the dynamic response of monolithic and cracked concrete gravity dams to dominant pulses of near-fault excitations. Zou et al. (2017) compared the dynamic behavior of high concrete face rockfill dams subjected to pulse-like and non-pulse ground motion.

In the study, it is aimed to determine the structural performance of concrete gravity dams under near- and far-

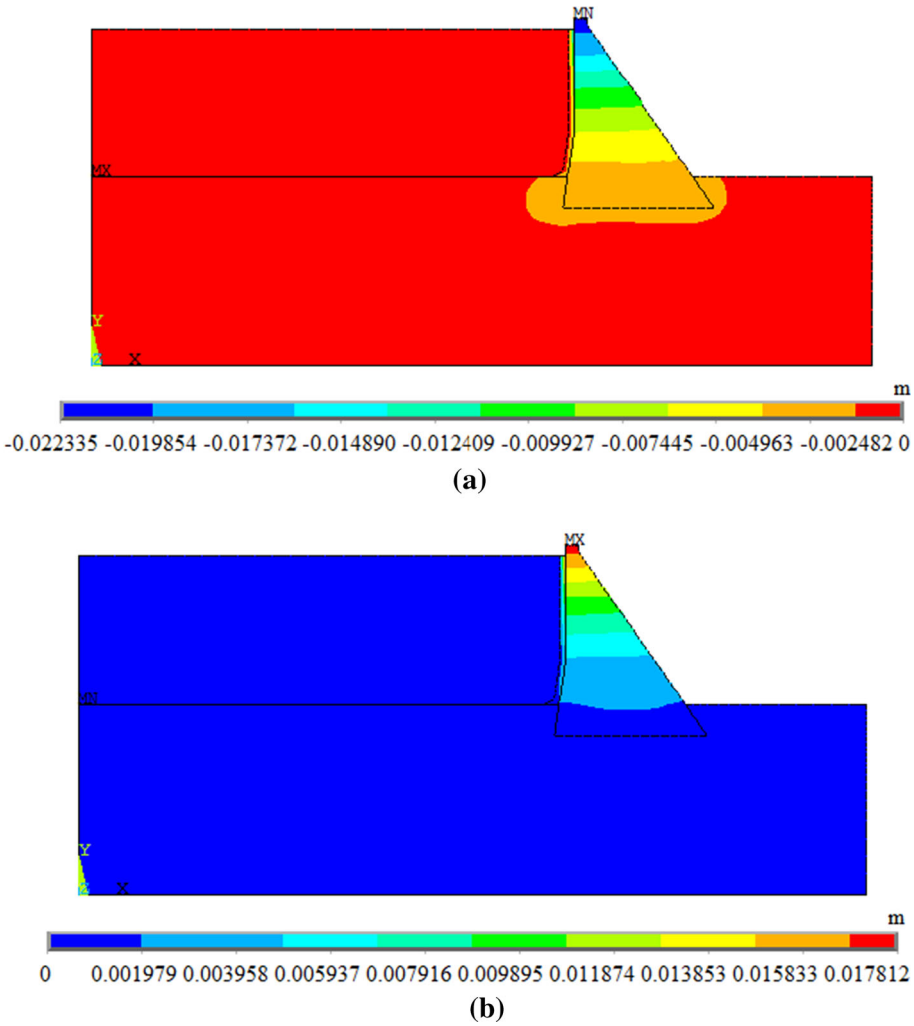

Fig. 7 Maximum displacement contour diagrams of the dam-reservoir-foundation system for near-fault (**a**) and far-fault records (**b**) of 1987 Superstition Hills (B) earthquake

fault ground motions using Euler water modeling approach. Sarıyar concrete gravity dam is selected as a case study. Three different earthquake records having approximately the same peak ground acceleration are utilized to represent near- and far-fault ground motion excitations. Linear transient analyses of Sarıyar concrete gravity dam are conducted subjected to near- and far-fault ground motions.

2 Near- and Far-Fault Ground Motions

The effect of a traveling wave on a structure depends on many factors such as wave traveling, wave pattern and structural dynamic. Properties of ground motions are among them. The characteristic of pulse either in acceleration time history or in velocity time history of near-fault ground motions is distinguished from far field ground motions (Yan and Lee 2007). So, the characteristics of ground motions play an important role on the structural performance of engineering structures, especially concrete gravity dams.

Near-fault ground motions are characterized by the long-period (Tp) pulses with high peak ground velocity. It produces high input energy on structures in the beginning of the earthquake. These pulses are strongly influenced by the orientation of the fault, the direction of slip on the fault and the location of the recording station relative to the fault, which is termed as 'directivity effect' due to the propagation of the rupture toward the recording site.

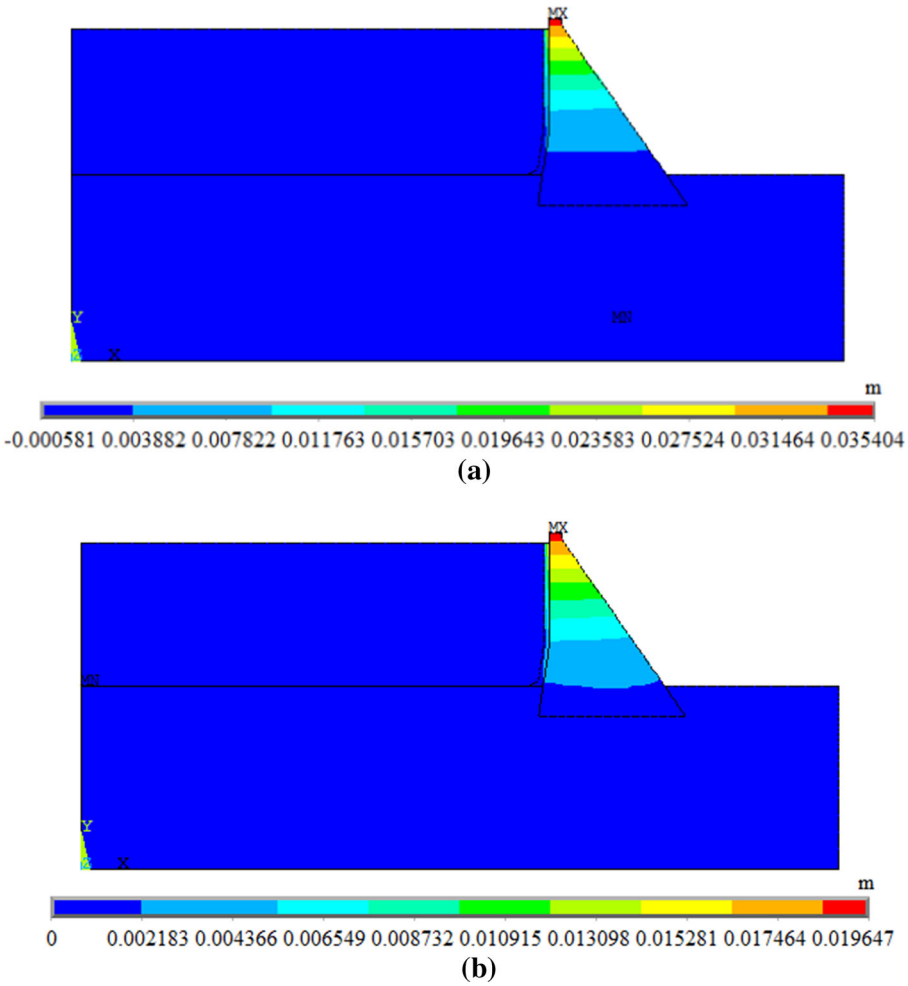

Fig. 8 Maximum displacement contour diagrams of the dam-reservoir-foundation system for near-fault (**a**) and far-fault records (**b**) of 1989 Loma Prieta earthquake

Selection of near-fault ground motion records is very important and based on some special rules (i) distance of near-fault ground motion record is less than 10 km, (ii) velocity pulse duration in near-fault ground motions is larger than 1.0 s, (iii) ratio of peak ground velocity (PGV) to peak ground acceleration (PGA) is larger than 0.1 s.

In this study, near-fault ground motion records are selected as an input motion from 1987 Superstition Hills (B), 1989 Loma Prieta and 1994 Northridge earthquakes. These records are taken from station numbers PTS225, CLS090 and RR318, respectively. In addition, another set of earthquake records, which recorded the same site conditions from the same earthquakes' events with epicenter far away from the site, is selected to illustrate far-fault ground motion characteristics. These records are taken from station numbers POE270, CYC285 and STN20, respectively.

Peak ground acceleration (PGA) and peak ground velocity (PGV), surface projection distances from the site to the fault and PGV/PGA values for selected ground motion records are given in Table 1. The records are attained from the PEER strong motion database (PEER 2013). To compare the analysis results more accurately, it is aimed to select near- and far-fault ground motion records with same peak acceleration values of each earthquake. The acceleration and velocity time histories of near- and far-fault ground are shown in Figs. 1 and 2, respectively. It can be easily seen from the figures that the velocity pulses of near-fault ground motions are significantly different as compared to far-fault ground motions. The near-fault

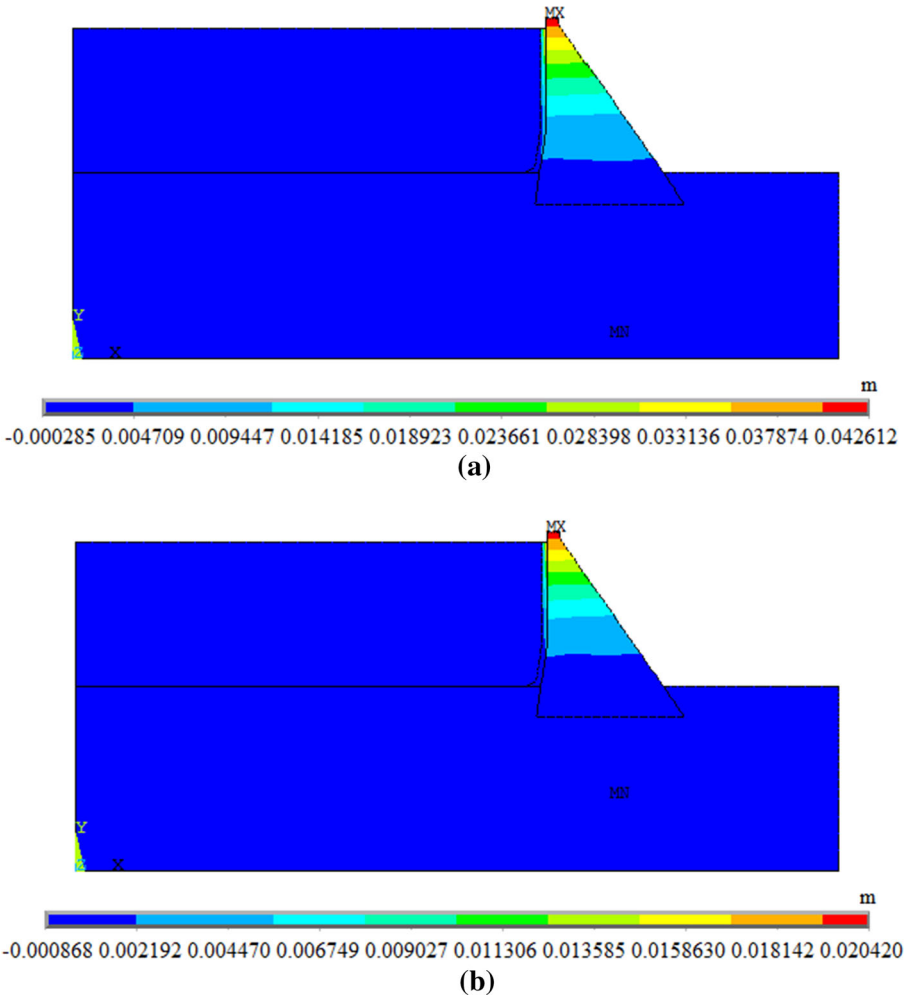

Fig. 9 Maximum displacement contour diagrams of the dam–reservoir–foundation system for near-fault (**a**) and far-fault records (**b**) of 1994 Northridge earthquake

ground motions have significantly long-period velocity pulses.

3 Formulation of Dam–Reservoir–Foundation Interaction

Dams are named as a group of structures subjected to fluid–structure interaction. So, the response of the fluid and its hydrodynamic pressures on the dam should be reflected more accurately in the structural analyses to determine the real behavior as soon as possible. Different mathematical and analytical modeling approaches can be used to calculate the water hydrodynamic pressure effect on the dam body.

In the Westergaard approach (added mass approach), the dam is accepted as rigid, semi-infinite and has vertical upstream surface. Surface waves in fluid are neglected. The distribution of hydrodynamic pressure occurred along upstream surface after earthquake is taken into account as mass distribution pulsed with the dam. Individual masses calculated with distribution of hydrodynamic pressure are added on the nodes of the finite element mesh along upstream surface of the dam.

In the Lagrange approach, the response of the dam and reservoir is expressed with displacements. For using the same variables, specific interface equations are not essential. In this approach, the fluid is assumed to be linearly elastic, inviscid and with irrotational flow field.

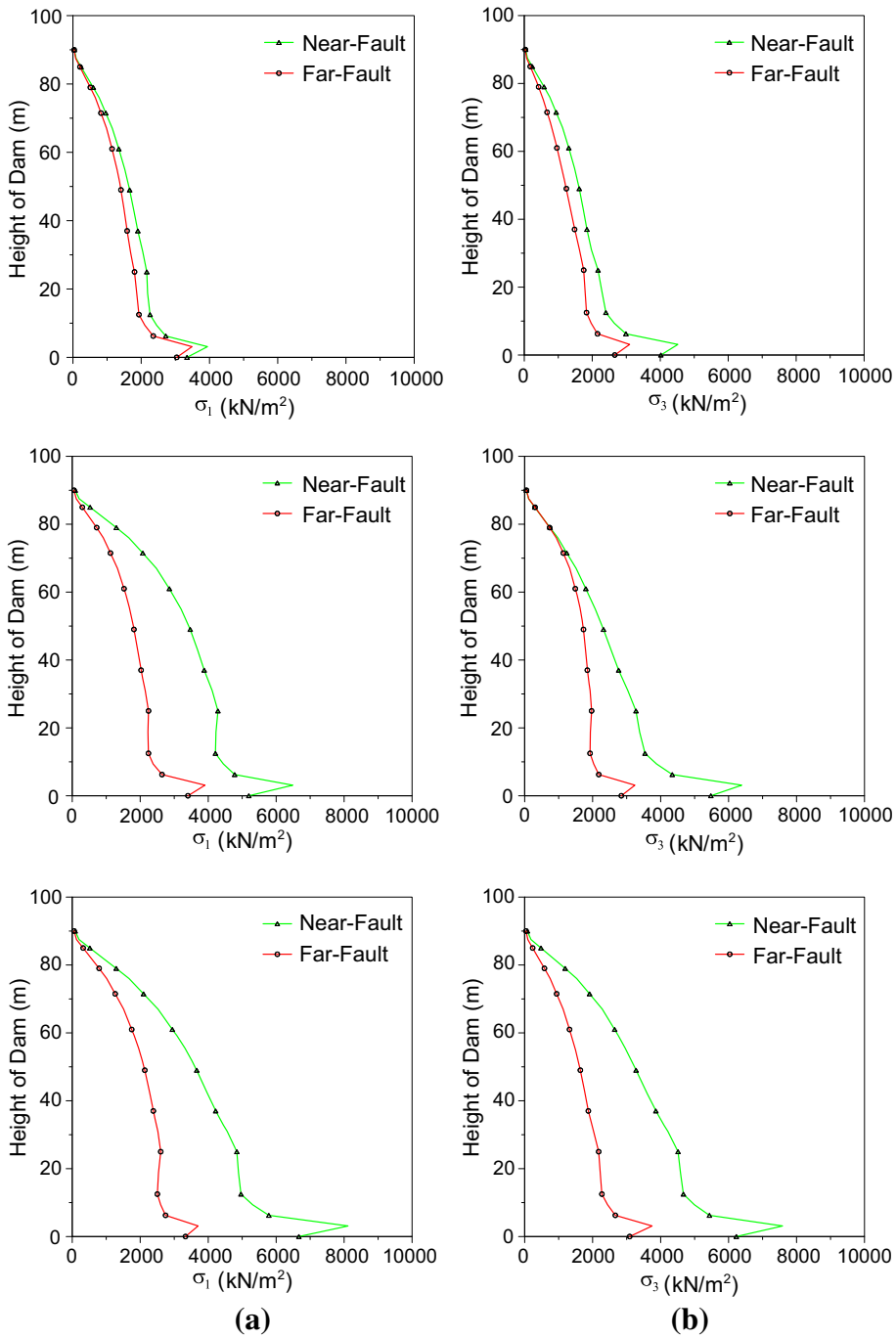

Fig. 10 Change in maximum tensile (**a**) and compressive (**b**) principal stresses by height of the Sarıyar concrete gravity dam subject to 1987 Superstition Hills (B), 1989 Loma Prieta and 1994 Northridge earthquakes

Euler approach is widely used in the finite and boundary element analysis for dams considering fluid–structure interaction. In this approach, the structure and fluid motions are expressed with displacements and pressures, respectively. Structure and fluid move together based on fluid–structure interface. Hence, specific interface equations must be identified as in this study.

The formulations of fluid system based on the Eulerian approach have been presented in many studies (Cook et al. 1989; Zeinkiewicz and Taylor 1991; Chopra 1967; Altunisik and Sesli 2015).

4 Numerical Example

The focus of this paper is to evaluate and compare the structural responses of concrete gravity dams under near- and far-fault ground motions. Sarıyar concrete gravity dam (Fig. 3a) is chosen as an application. The dam is located on

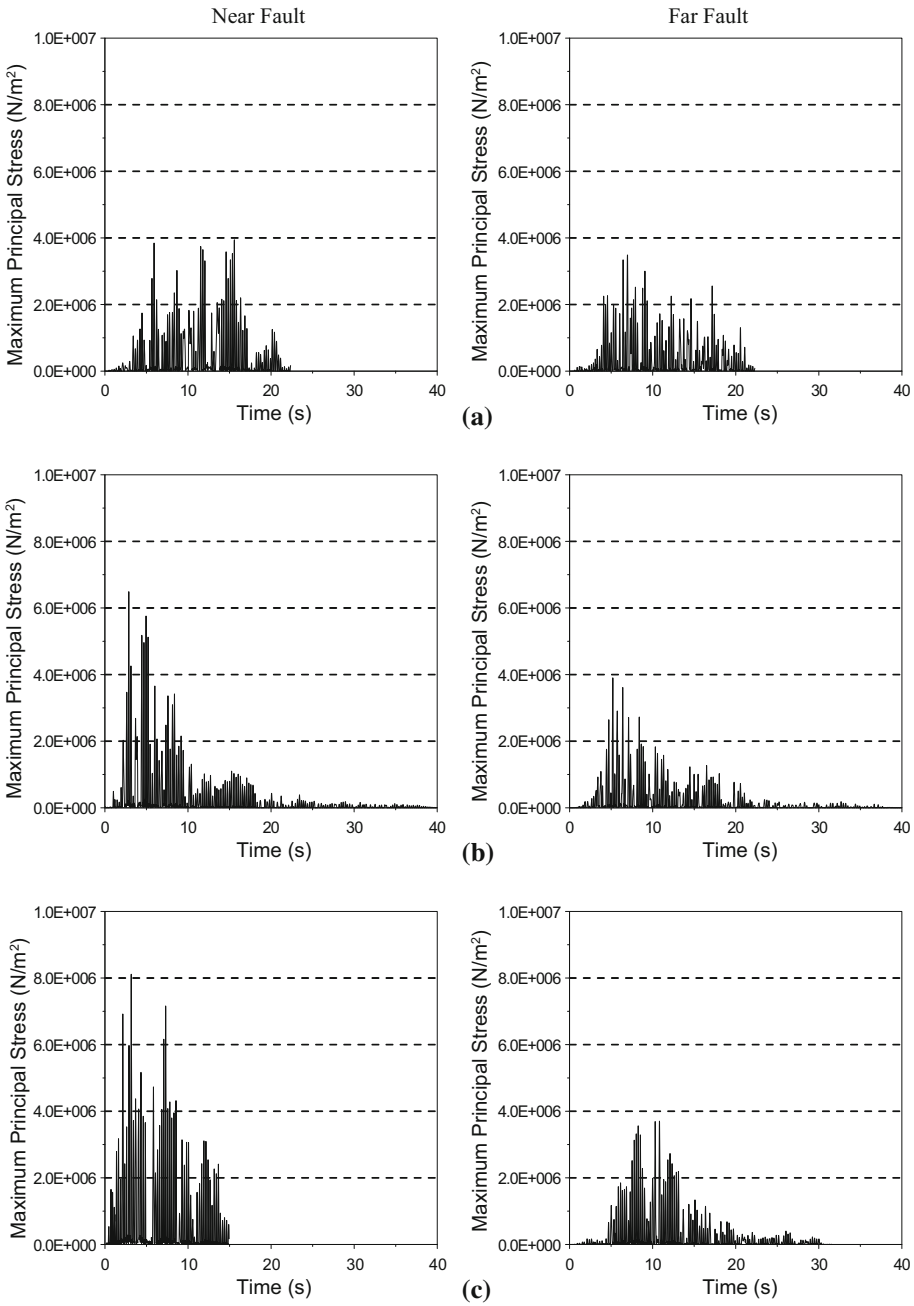

Fig. 11 Time histories of maximum principle stresses at the 3.125 m for **a** 1987 Superstition Hills (B), **b** 1989 Loma Prieta and **c** 1994 Northridge earthquakes

the Sakarya River, 120 km to the northeast of Ankara, in Turkey. The dam was constructed to supply the electric power. The crest length and width are 257 and 7 m, respectively. Maximum reservoir height is 85 m. The dimensions of the dam are given in Fig. 3b.

The finite element model of the dam including dam–reservoir–foundation interaction using Euler approach is constituted in ANSYS program (Fig. 4). In the model, dam body and foundation are represented by solid elements. Reservoir effect is represented by using fluid elements to define the reservoir water and its hydrodynamic pressures.

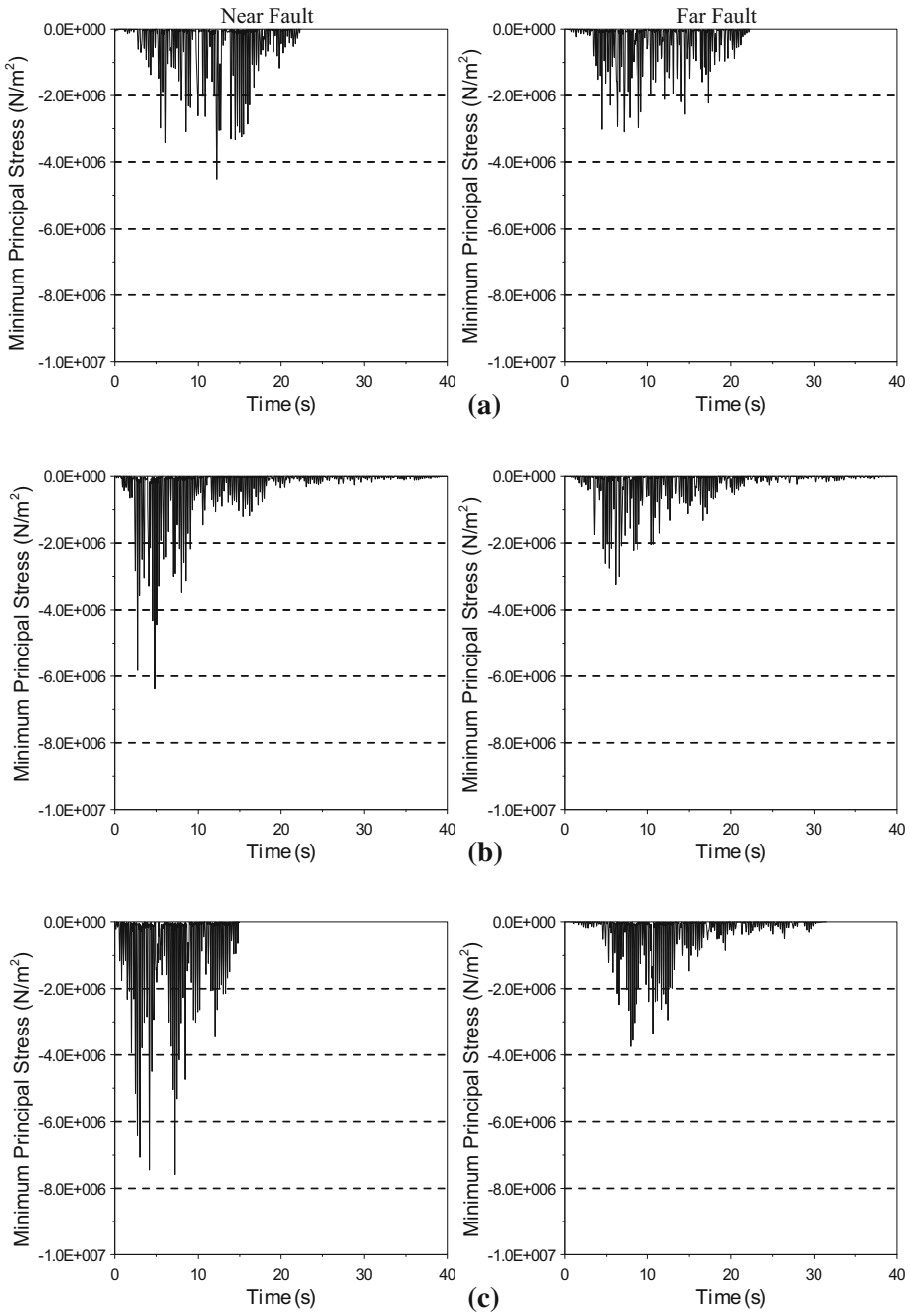

Fig. 12 Time histories of minimum principle stresses at the 3.125 m for **a** 1987 Superstition Hills (B), **b** 1989 Loma Prieta and **c** 1994 Northridge earthquakes

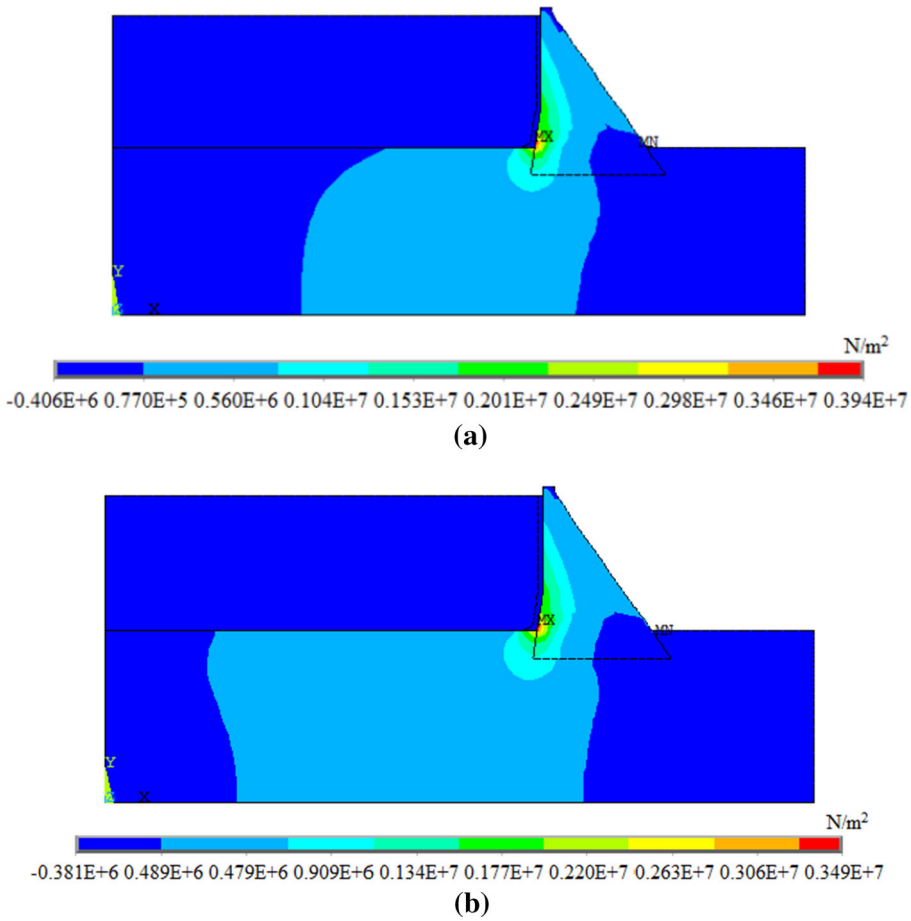

Fig. 13 Maximum tensile stresses contours for near-fault (**a**) and far-fault (**b**) records considering 1987 Superstition Hills (B) earthquake

Plane182 element is used for dam body and foundation. Also, Fluid29 (structure absent) elements are selected to represent the reservoir water.

The finite element method can be applied with many idealizations for soil and structure which represents infinite soil media as a finite and bounded media. The encountered numerical problem in dynamic soil-structure interaction analysis with the method is how to simulate waves that radiate outward from the excited structures toward infinity. The dynamic response of massive structures such as nuclear power plants and dams may be influenced by the soil-structure interaction as well as the dynamic characteristics of the exciting loads and the structures. To model the infinite soil media, a radiation condition at infinity has to be satisfied. Various boundary conditions were developed by researchers for soil-structure interaction systems (Astley 2000). If special boundary conditions are not used for soil media, use of massless foundation can be a significant solution for soil-structure interaction problems (Dumanoglu 1980).

Massless foundation is used in the dam-reservoir-foundation model. Between the dam and reservoir faces, the thickness of Fluid 29 element is chosen as 3.125 m for Euler approach. The length of the reservoir in the upstream direction is taken to be as much as three times the dam height in all models. In addition, foundation depths are taken into account as much as the dam heights. In the upstream direction, foundation length is considered as the reservoir length, and in the downstream direction, foundation length is considered as the dam height. Element matrices are computed using the Gauss numerical integration technique (Bathe 1996). The Newmark method is used in the solution of the equation of motions. Rayleigh damping is considered in the analyses, and damping ratio is selected as 5%. The material properties used in the analyses are given in Table 2.

4.1 Displacements

The time histories of the horizontal displacements (upstream–downstream directions) at the crest point of Sarıyar concrete gravity dam obtained from linear transient analysis for near- and far-fault ground motion considered 1987 Superstition Hills (B), 1989 Loma Prieta and 1994 Northridge earthquakes are presented Fig. 5a–c. The maximum displacements are attained as 22.34–17.81, 35.40–19.64 and 42.61–20.42 mm for near fault and far fault, respectively.

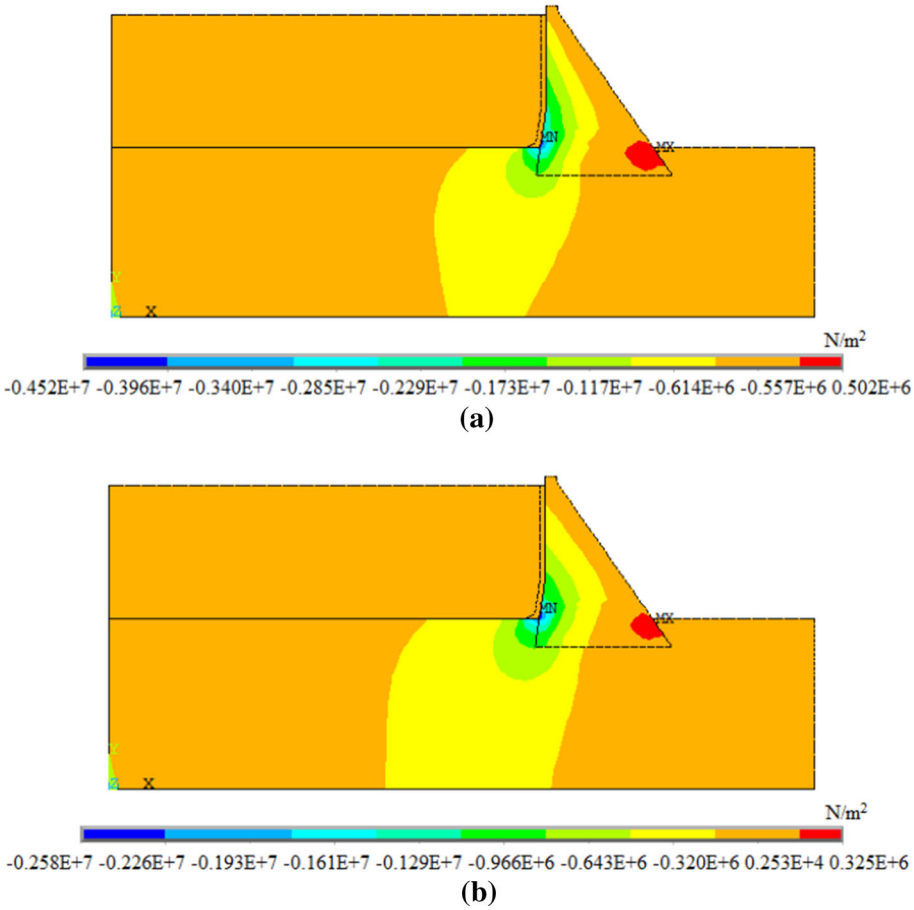

Fig. 14 Maximum compressive stresses contours for near-fault (**a**) and far-fault (**b**) records considering 1987 Superstition Hills (B) earthquake

The change in maximum displacements by the height of dam body is given in Fig. 6a–c. It is clearly seen that the displacements increase by height of the dam body and maximum displacements attained for near-fault ground motions. The maximum horizontal displacements contour diagrams for all ground motions are shown in Figs. 7, 8 and 9a, b. This represents the distribution of the peak values reached by the maximum displacement at each point within the sections. It can be seen that near-fault ground motions more effective than far-fault ground motions on displacements.

4.2 Principal Stresses

The change in maximum compressive and tensile principal stresses by the height of dam body for near- and far-fault ground motions in given in Fig. 10a, b. It is seen that the maximum values of both principle stresses are attained at 3.215 m height from the base point of the dam body. The time histories of the principal stresses (at 3.125 m) are plotted in Figs. 11a–c and 12a–c.

The maximum tensile stresses are attained as 3.94–3.49, 6.49–3.90 and 8.11–3.70 MPa; the maximum compressive stresses are attained as 4.52–3.10, 6.39–3.24 and 7.59–3.75 MPa for near- and far-fault ground motion records considering 1987 Superstition Hills (B), 1989 Loma Prieta and 1994 Northridge earthquakes, respectively. The maximum stresses contour diagrams are shown in Figs. 13, 14, 15, 16, 17 and 18a, b. This represents the distribution of peak values reached by maximum stresses at each point within the sections.

4.3 Principal Strains

The change in maximum compressive and tensile principal strains by the height of dam body for near- and far-fault ground motions is given in Fig. 19a–c. It is seen that the maximum values of both principle strains are attained at 3.215 m height from the base point of the dam body. The time histories of the principal strains (at 3.125 m) are plotted in Figs. 20 and 21a–c. The maximum tensile and compressive strains are attained as (11.09E−5)–(98.12E−6), (18.23E−5)–(10.98E−5) and (22.80E−5)–(10.42E−5); (12.71E−5)–(87.11E−6), (17.96E−5)–(91.25E−6) and (21.33E−5)–(10.54E−5) for near fault and far fault, respectively. The maximum strain contours are shown in Figs. 22, 23, 24, 25, 26 and 27a, b.

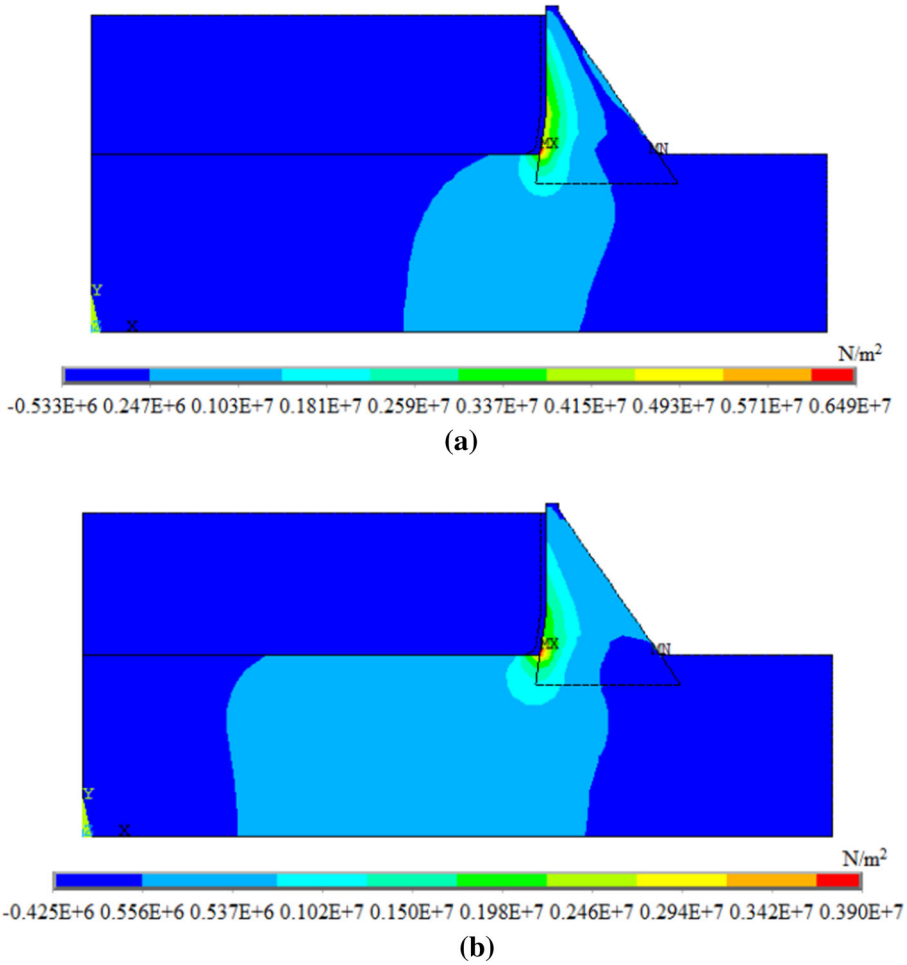

Fig. 15 Maximum tensile stresses contours for near-fault (**a**) and far-fault (**b**) records considering 1989 Loma Prieta earthquake

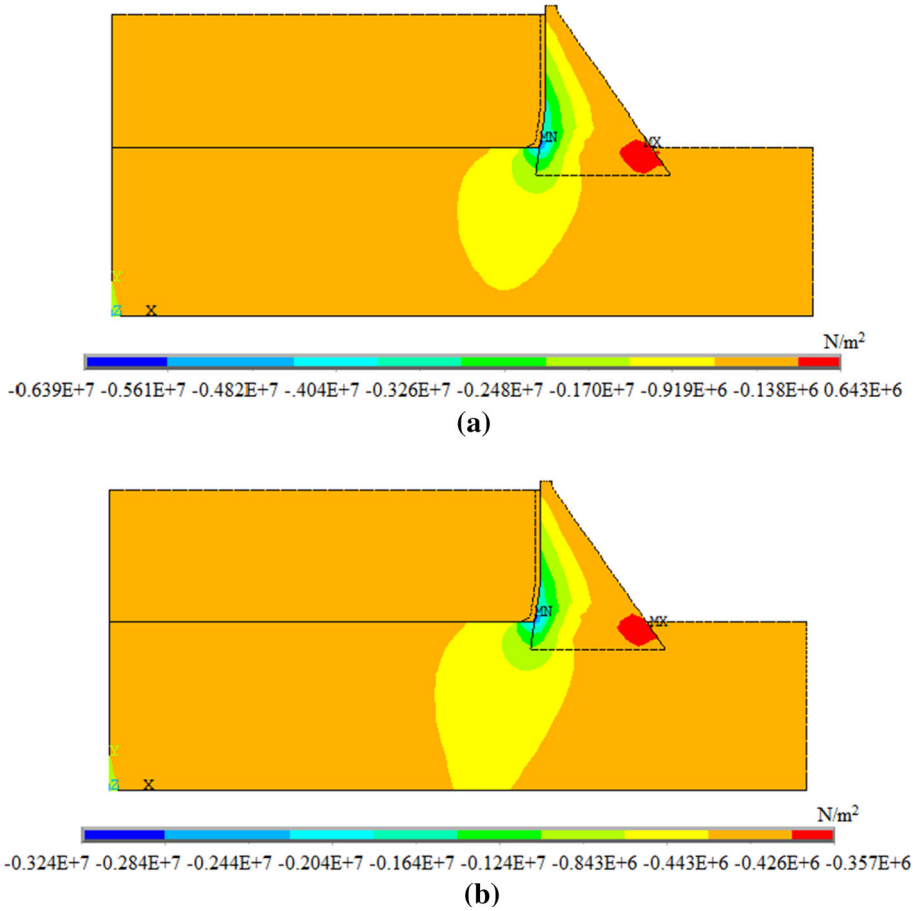

Fig. 16 Maximum compressive stresses contours for near-fault (**a**) and far-fault (**b**) records considering 1989 Loma Prieta earthquake

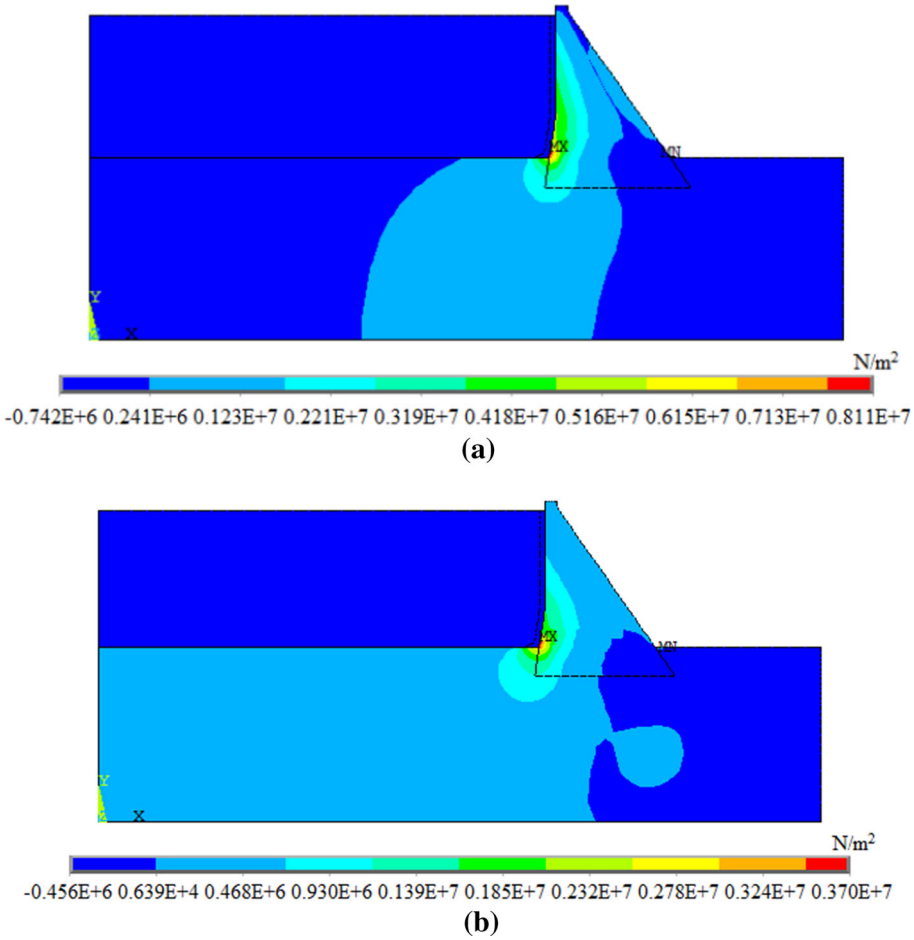

Fig. 17 Maximum tensile stresses contours for near-fault (**a**) and far-fault (**b**) records considering 1994 Northridge earthquake

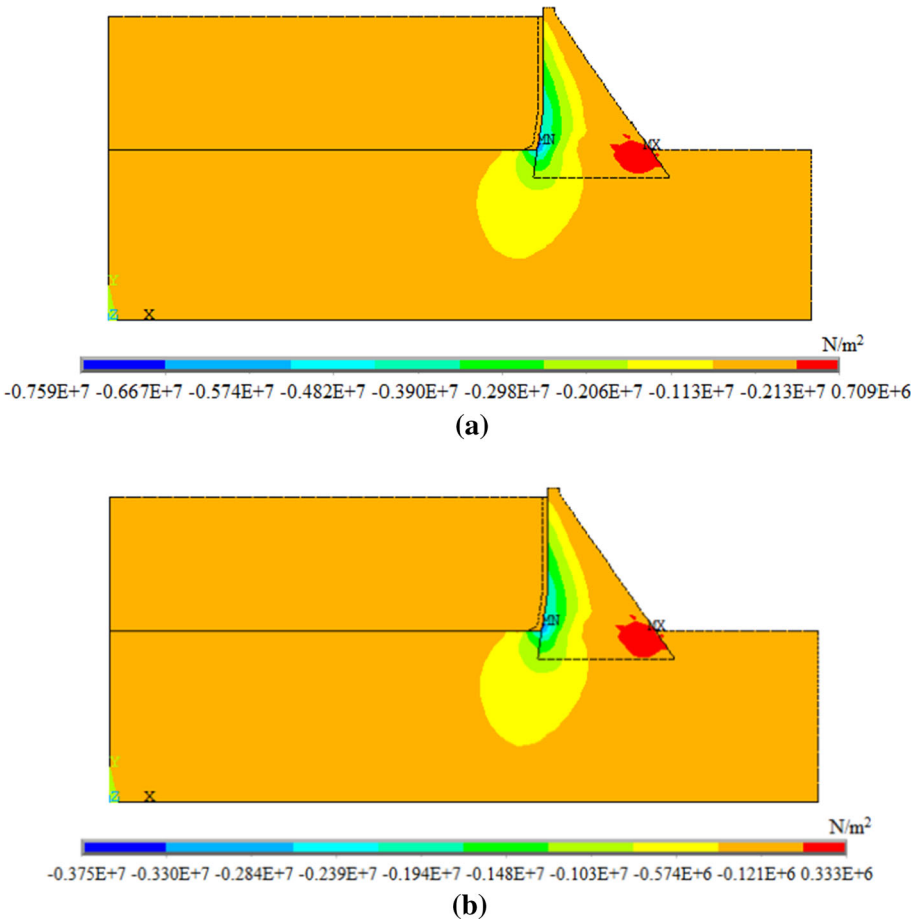

Fig. 18 Maximum compressive stresses contours for near-fault (**a**) and far-fault (**b**) records considering 1994 Northridge earthquake

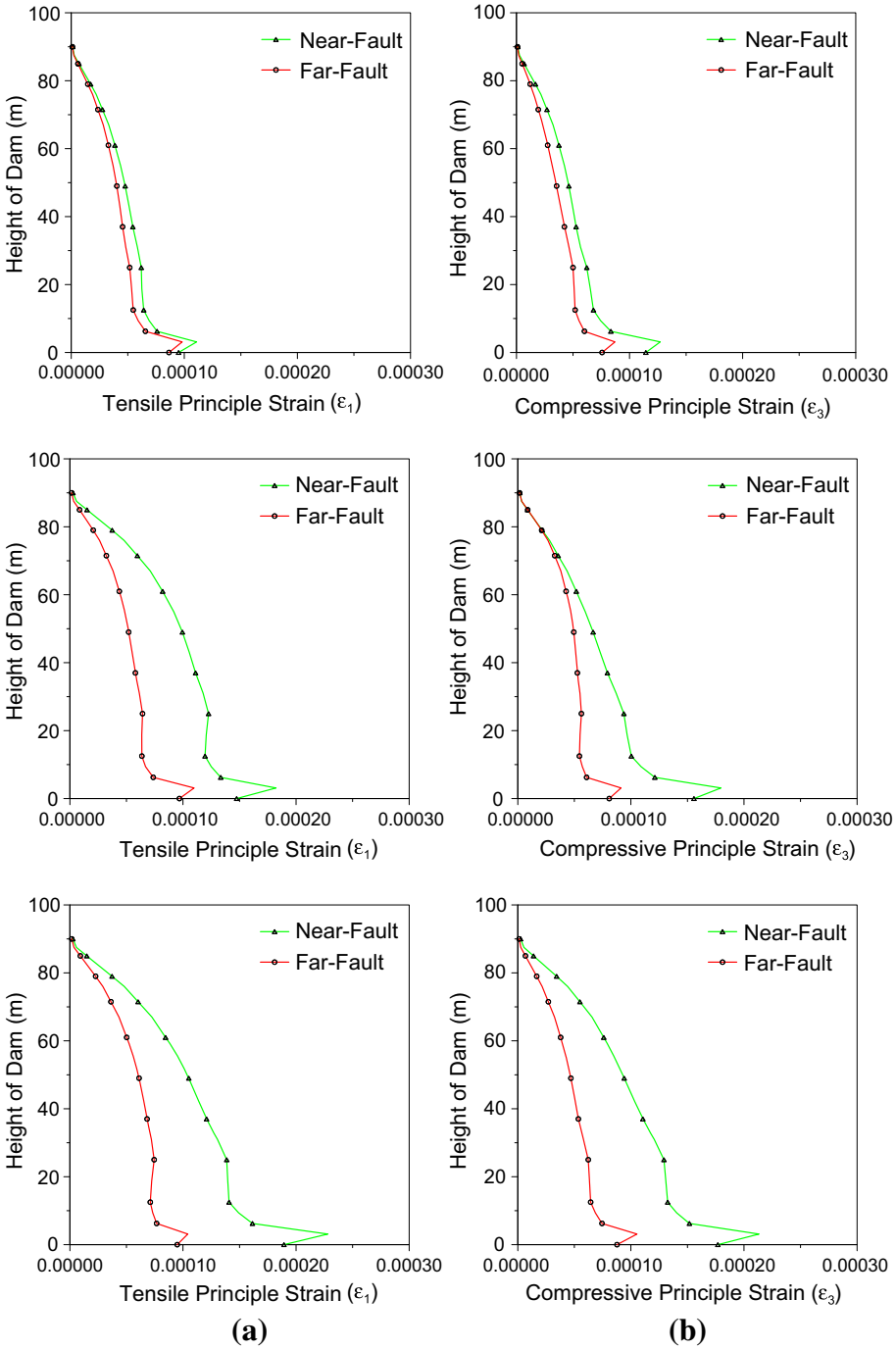

Fig. 19 Change in maximum tensile (**a**) and compressive (**b**) principal stresses by height of the Sarıyar concrete gravity dam for 1987 Superstition Hills (B), 1989 Loma Prieta and 1994 Northridge earthquakes

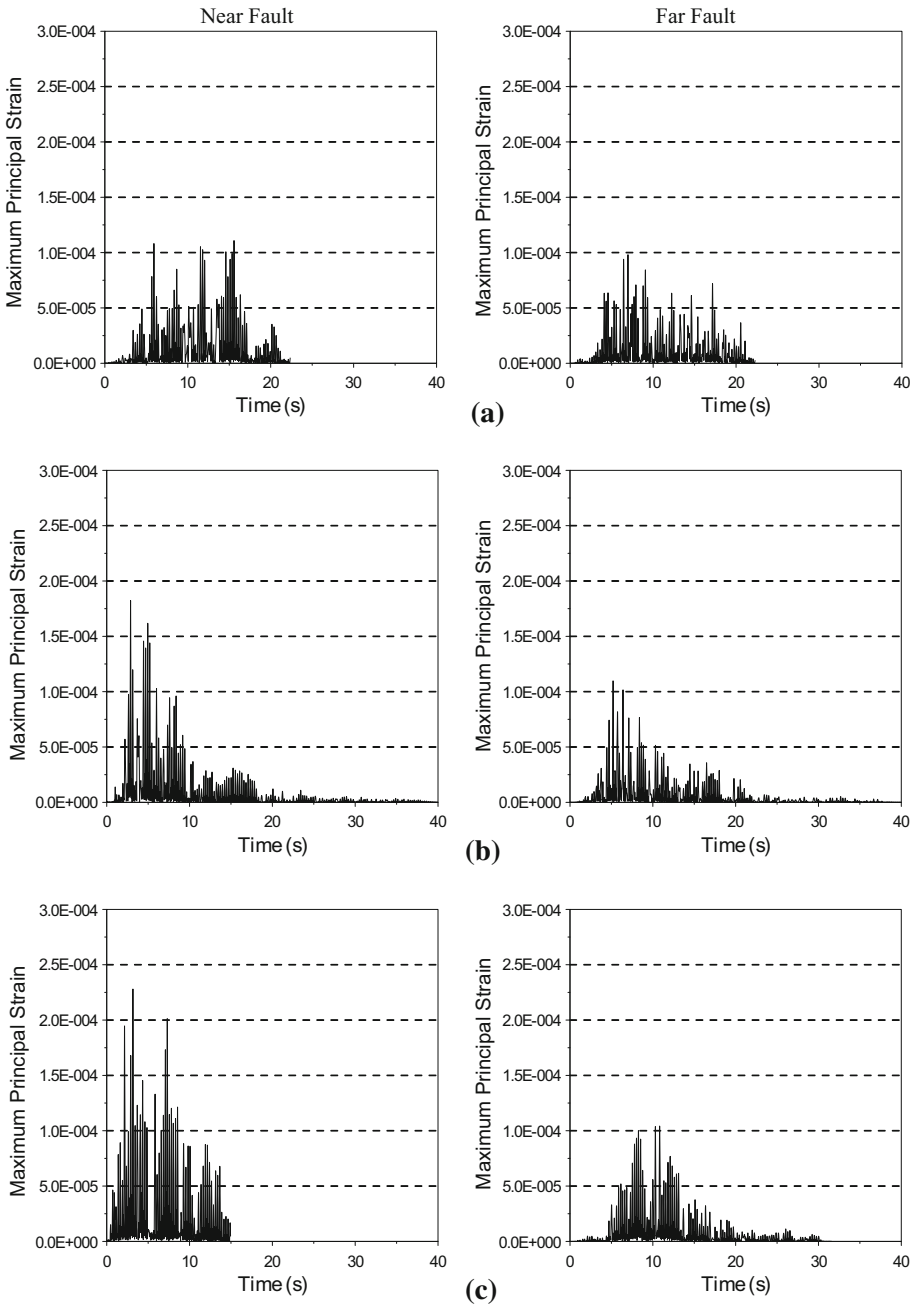

Fig. 20 Time histories of maximum principle strains at the 3.125 m for **a** 1987 Superstition Hills (B), **b** 1989 Loma Prieta and **c** 1994 Northridge earthquakes

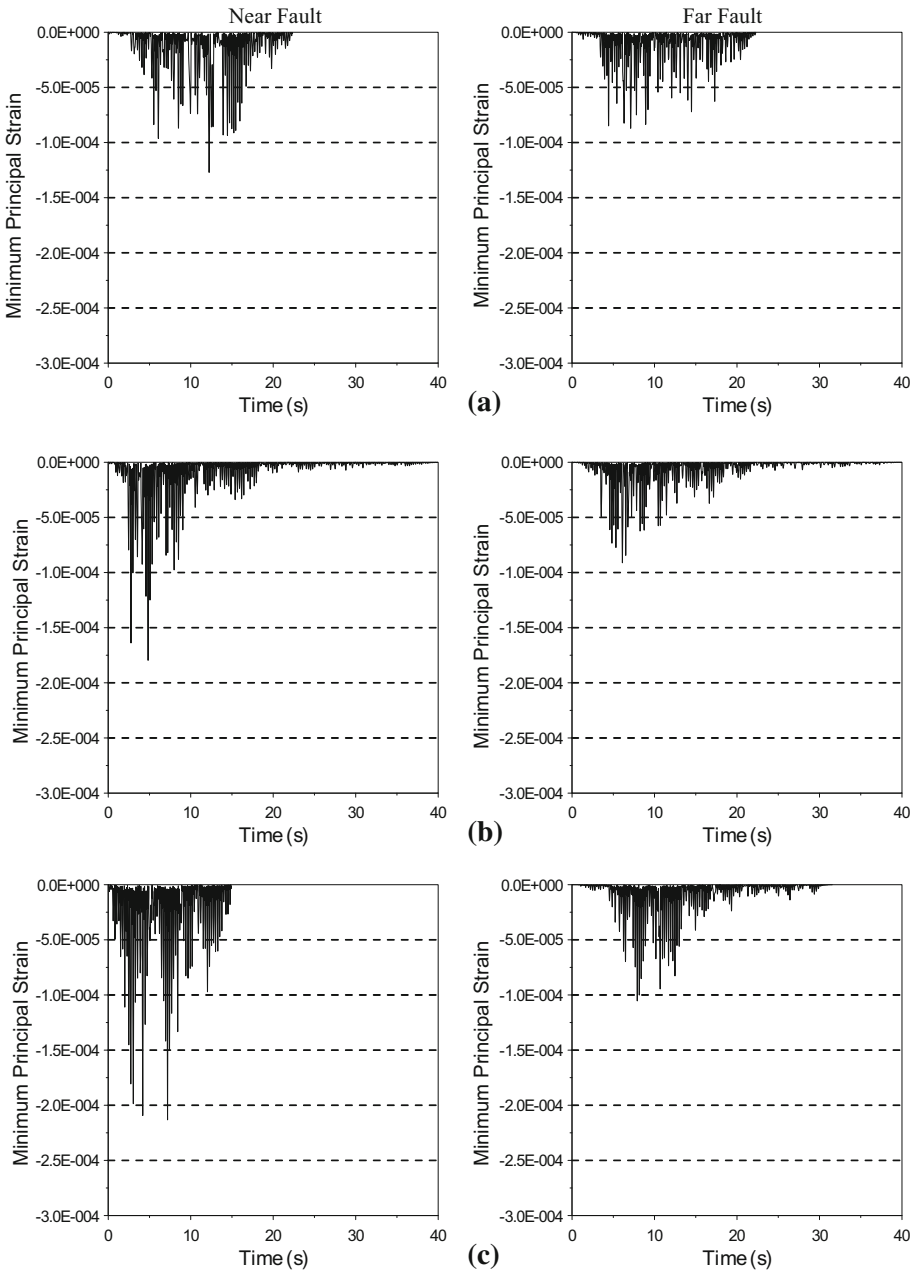

Fig. 21 Time histories of minimum principle strains at the 3.125 m for **a** 1987 Superstition Hills (B), **b** 1989 Loma Prieta and **c** 1994 Northridge earthquakes

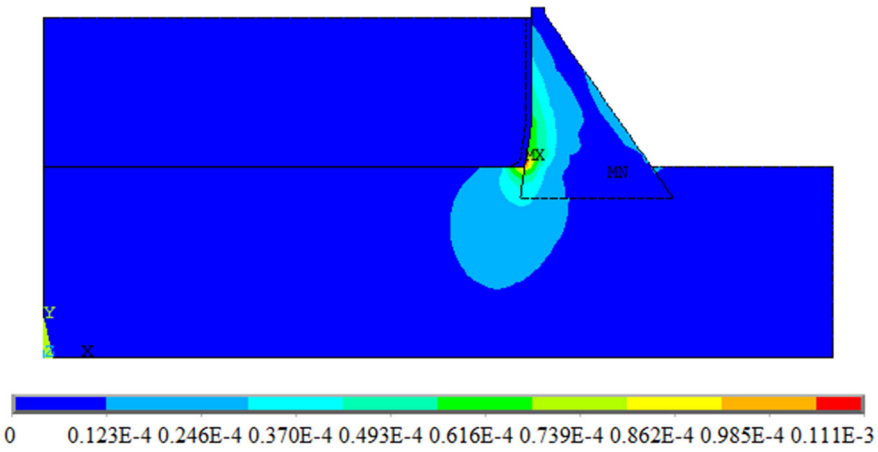

(a)

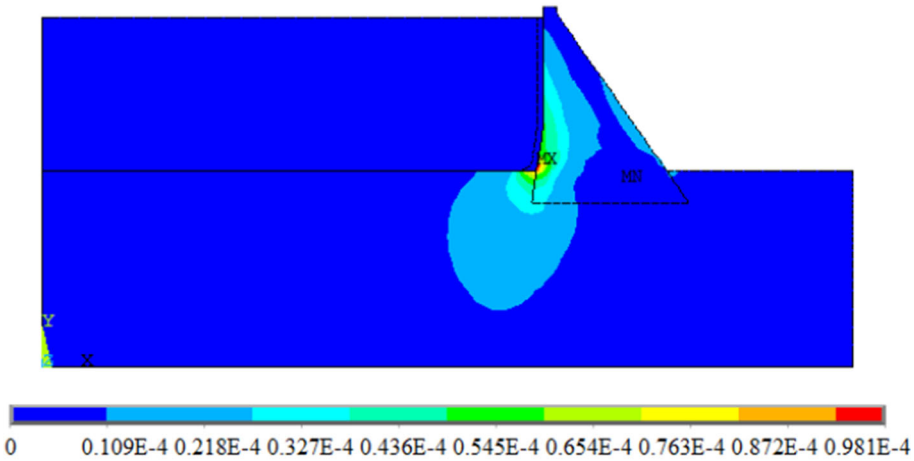

(b)

Fig. 22 Maximum tensile strain contour diagrams of the dam–reservoir–foundation system for near-fault (**a**) and far-fault records (**b**) of 1987 Superstition Hills (B) earthquake

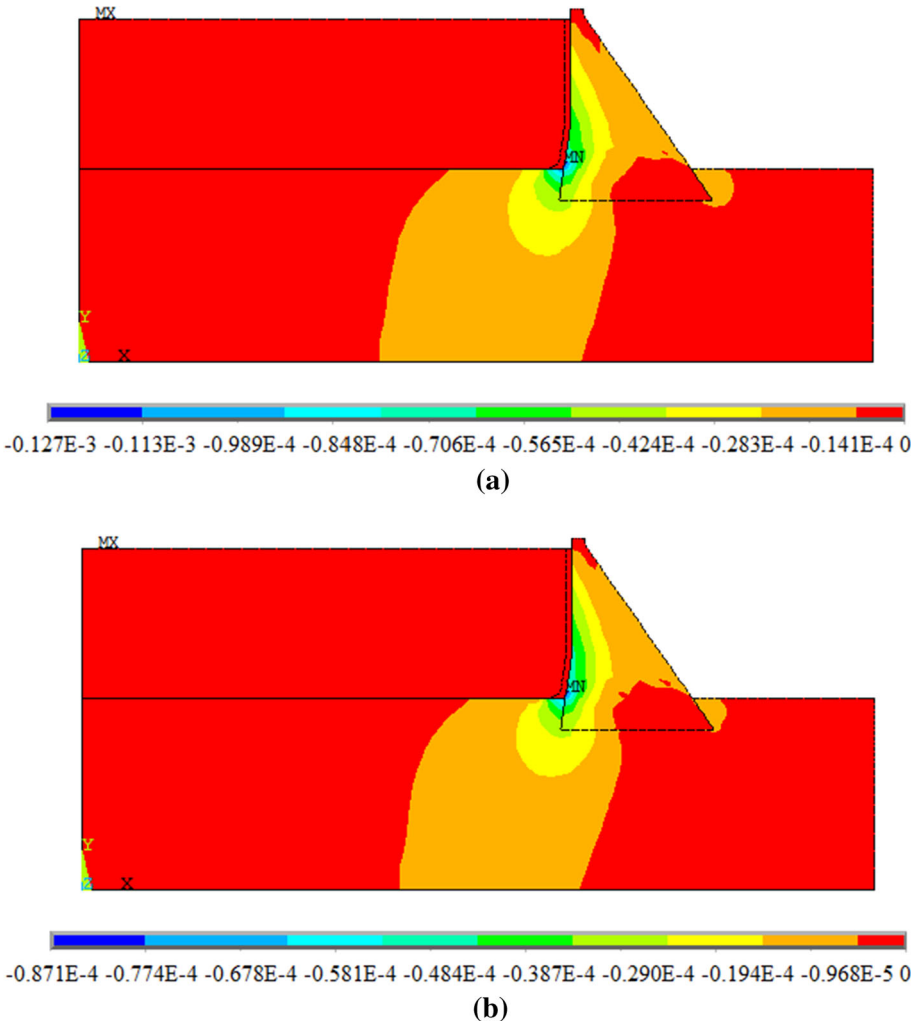

Fig. 23 Maximum compressive strain contour diagrams of the dam–reservoir–foundation system for near-fault (**a**) and far-fault records (**b**) of 1987 Superstition Hills (B) earthquake

5 Conclusions

To evaluate the structural performance of concrete gravity dams subjected to near- and far-fault ground motions, linear transient analyses are performed under three different earthquake records which have approximately same peak ground acceleration. The selected near- and far-fault earthquake records are applied on two-dimensional finite element model of Sarıyar concrete gravity dam which is 120 km to the northeast of Ankara, Turkey. Eulerian approach was chosen for fluid–structure interaction.

Results of analyses show that the displacements increase along the height of the dam for all ground motions. Maximum and minimum principal stresses and strains have a decreasing trend along the height of the dam from bottom (3.125 m height from the base point of the dam body) to top of the dam. Moreover, the maximum tensile and compressive stresses and strains are obtained at 3.125 m height from the base point of the dam body.

Although chosen near- and far-fault ground motions have same peak ground acceleration, the maximum values are attained from near-fault motions. Also, the analysis using near-fault ground motion of 1994 Northridge earthquake gives the maximum of the maximum values.

It is seen from the analyses that under near-fault ground motions of 1989 Loma Prieta and 1994 Northridge earthquakes two time values are given than far-fault ground motions of the same earthquakes. But differences between values obtained near- and far-fault ground motions for 1987 Superstition Hills (B) are substantially lower. It can be explained as near-fault ground motion pulse effect.

It can be indicated that maximum values for concrete gravity dams such as displacements, stresses and strains have not been obtained even if ground motions have peak acceleration values.

It can be easily seen that near-fault ground motions have a remarkable effect on the structural performance of concrete gravity dams. So, near-fault ground motions should be taken into account to obtain more realistic results for

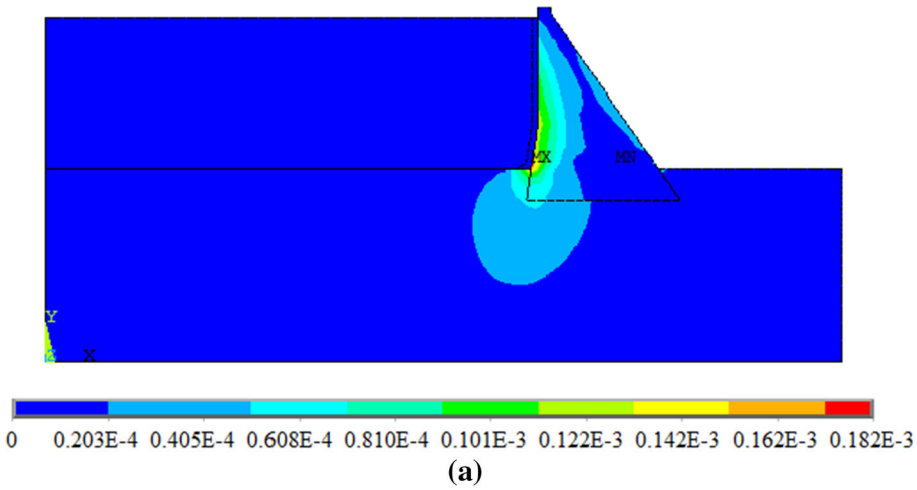

Fig. 24 Maximum tensile strain contour diagrams of the dam–reservoir–foundation system for near-fault (**a**) and far-fault records (**b**) of 1987 Superstition Hills (B) earthquake

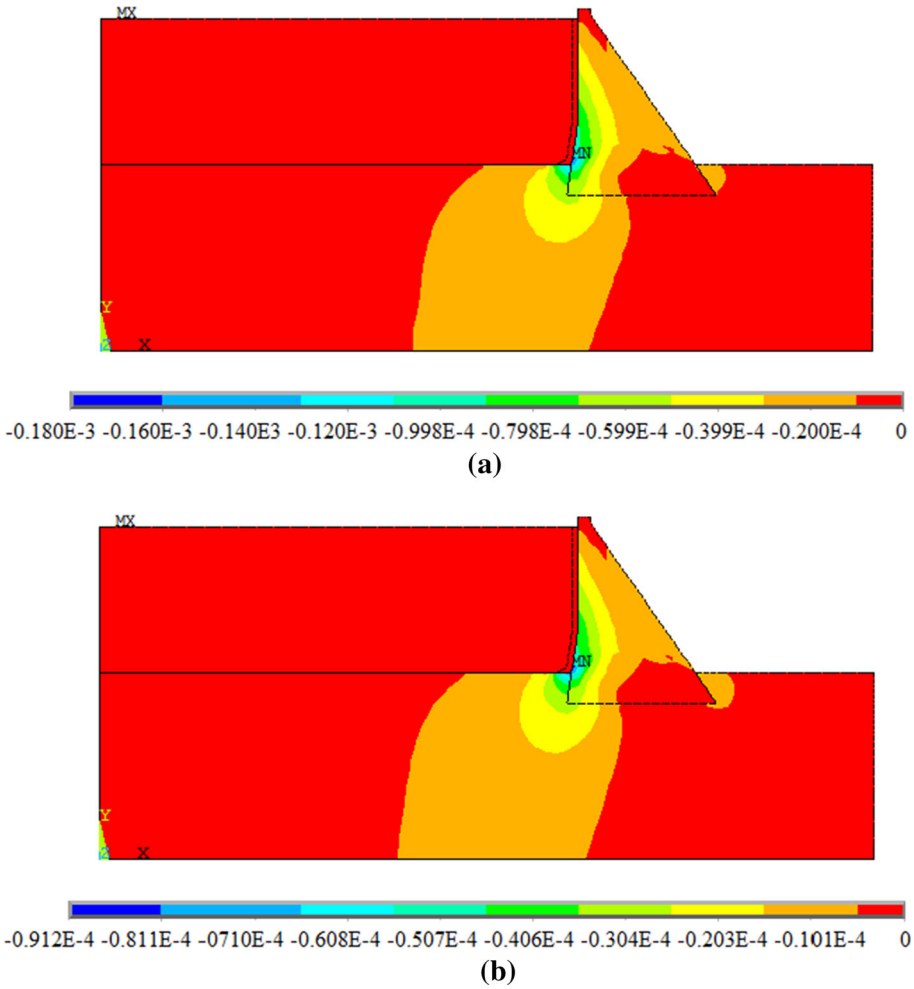

Fig. 25 Maximum compressive strain contour diagrams of the dam-reservoir-foundation system for near-fault (**a**) and far-fault records (**b**) of 1989 Loma Prieta earthquake

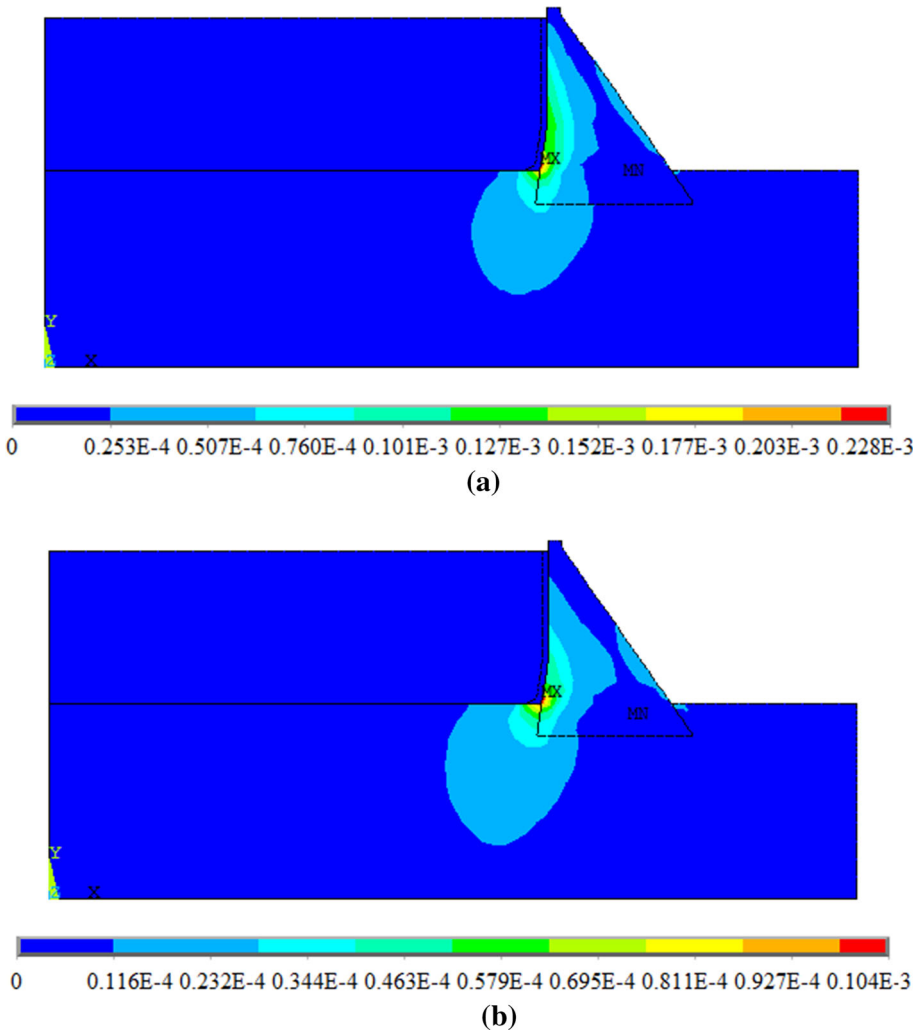

Fig. 26 Maximum tensile strain contour diagrams of the dam-reservoir-foundation system for near-fault (**a**) and far-fault records (**b**) of 1994 Northridge earthquake

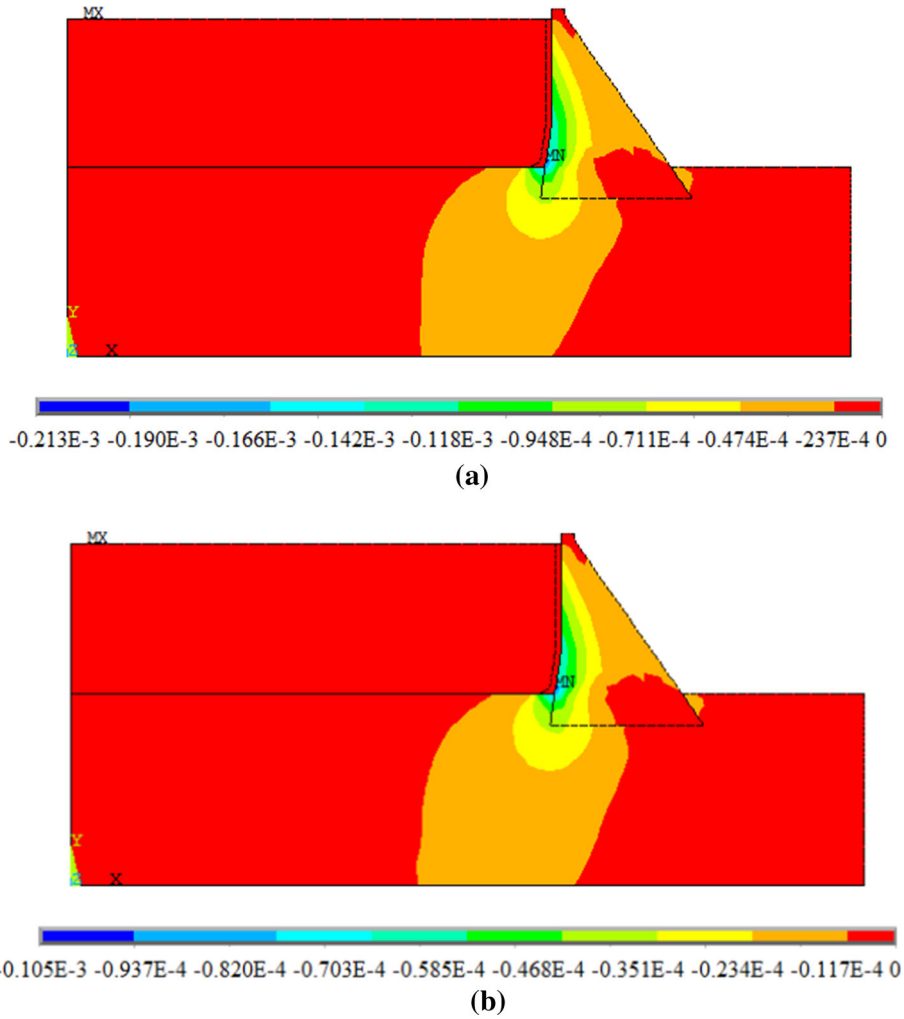

Fig. 27 Maximum compressive strain contour diagrams of the dam-reservoir-foundation system for near-fault (**a**) and far-fault records (**b**) of 1994 Northridge earthquake

concrete gravity dams in the design and restoration phases. Also, in the further studies, near-fault ground motion pulse effect on the dynamic behavior of gravity dam–reservoir–foundation systems should be taken into account.

References

Adanur S, Altunişik AC, Bayraktar A, Akköse M (2012) Comparison of near-fault and far-fault ground motion effects on geometrically nonlinear earthquake behavior of suspension bridges. Nat Hazards 64:593–614. https://doi.org/10.1007/s11069-012-0259-5

Akköse M, Şimşek E (2010) Non-linear seismic response of concrete gravity dams to near-fault ground motions including dam–water–sediment–foundation interaction. Appl Math Model 34:3685–3700. https://doi.org/10.1016/j.apm.2010.03.019

Alavi B, Krawinkler H (2000) Consideration of near-fault ground motion effects in seismic design. In: Proceedings of the 12th world conference of earthquake engineering, New Zealand, Paper No. 2665

Alavi B, Krawinkler H (2004) Strengthening of moment-resisting frame structures against near-fault ground motion effects. Earthq Eng Struct Dyn 33:707–722. https://doi.org/10.1002/eqe.370

Altunisik AC, Sesli H (2015) Dynamic response of concrete gravity dams using different water modelling approaches: Westergaard, Lagrange and Euler. Comput Concr 16(3):429–448. https://doi.org/10.12989/cac.2015.16.3.429

Amiri FS, Amiri GG, Razeghi H (2013) Estimation seismic demands of steel frames subjected to near-fault earthquakes having forward directivity and comparing with pushover analysis results. Struc Des Tall Spec Build 22:975–988. https://doi.org/10.1002/tal.747

Antonellis G, Panagiotou M (2014) Seismic response of bridges with rocking foundations compared to fixed-base bridges at near-fault site. J Bridge Eng 19(5):04014007-1-13. https://doi.org/10.1061/(asce)be.1943-5592.0000570

Astley RJ (2000) Infinite elements for wave problems: a review of current formulations and an assessment of accuracy. Int J Numer Methods Eng 49(7):951–976. https://doi.org/10.1002/1097-0207(20001110)49:7

Bathe KJ (1996) Finite element procedures in engineering analysis. Prentice-Hall, Englewood Cliffs

Bayraktar A, Altunisik AC, Sevim B, Turker E, Bilici Y (2009) Comparison of near- and far-fault ground motion effect on the nonlinear response of dam–reservoir–foundation systems. Nonlinear Dyn 58:655–673

Beiraghi H, Kheyroddin A, Kafi MA (2016) Energy dissipation of tall core-wall structures with multi-plastic hinges subjected to forward directivity near-fault and far-fault earthquakes. Struct Des Tall Spec Build 25(15):801–820. https://doi.org/10.1002/tal.1284

Chopra AK (1967) Hydrodynamic pressures on dams during earthquake. J Eng Mech 93:205–223

Chopra AK, Chintanapakdee C (2001) Comparing response of SDF systems to near-fault and far-fault earthquake motions in the context of spectral regions. Earthq Eng Struct Dyn 30:1769–1789. https://doi.org/10.1002/eqe.92

Cook RD, Malkus DS, Plesha ME (1989) Concept and applications of finite element analysis. Wiley, Singapore

Corigliano M, Scandella L (2011) Seismic analysis of deep tunnels in near fault conditions in Southern Italy as case study. Bull Earthq Eng 9:975–995. https://doi.org/10.1007/s10518-011-9249-3

Dumanoglu AA (1980) The dynamic soil-structure interaction analysis of embedded structures with non-reflecting boundaries. Bull Tech Univ İstanbul 33(1):1

Gang W, Changhai Z, Shuang L, Lili X (2014) Effects of near-fault ground motions and equivalent pulses on large crossing transmission tower-line system. Eng Struct 77:161–169. https://doi.org/10.1016/j.engstruct.2014.08.013

Ghaffarzadeh H, Dehrod EA, Par HA (2015) Semi-active fuzzy control of structures subjected to near-fault ground motions having forward directivity and fling step using friction damping system with amplifying braces (fdsab). Iran J Sci Technol Trans Civ Eng 39(C2):299–317. https://doi.org/10.22099/IJSTC.2015.3136

Hall JF, Heaton TH, Halling MW, Wald DJ (1995) Near-source ground motion and its effects on flexible buildings. Earthq Spectra 11(4):569–605. https://doi.org/10.1193/1.1585828

Huang J (2015) Earthquake damage analysis of concrete gravity dams: modeling and behavior under near-fault seismic excitation. J Earthq Eng 19:1037–1085. https://doi.org/10.1080/13632469.2015.1027019

Ismail M, Rodellar J, Casas JR (2016) Seismic behavior of RNC-isolated bridges: a comparative study under near-fault, long-period, and pulse-like ground motions. Adv Mater Sci Eng 189:7045. https://doi.org/10.1155/2016/1897045

Jonsson MH, Bessason B, Haflidason E (2010) Earthquake response of a base-isolated bridge subjected to strong near-fault ground motion. Soil Dyn Earthq Eng 30:447–455. https://doi.org/10.1016/j.soildyn.2010.01.001

Karalar M, Padgett JE, Dicleli M (2012) Parametric analysis of optimum isolator properties for bridges susceptible to near-fault ground motions. Eng Struct 40:276–287. https://doi.org/10.1016/j.engstruct.2012.02.023

Liao WL, Loh C, Lee B (2004) Comparison of dynamic response of isolated and non-isolated continuous girder bridges subjected to near-fault ground motions. Eng Struct 26:2173–2183. https://doi.org/10.1016/j.engstruct.2004.07.016

MacRae GA, Mattheis J (2000) Three-dimensional steel building response to near-fault motions. J Struct Eng 126:117–126. https://doi.org/10.1061/(ASCE)0733-9445

Panchal VR, Jangid RS (2014) Behaviour of liquid storage tanks with variable curvature friction pendulum system (VCFPS) under near-fault ground motions. Struct Infrastruct Eng 8(1):71–88. https://doi.org/10.1080/15732470903300919

Park SW, Ghasemi H, Shen J, Somerville PG, Yen WP, Yashinsky M (2004) Simulation of the seismic performance of the Bolu Viaduct subjected to near-fault ground motions. Earthq Eng Struct Dyn 33:1249–1270. https://doi.org/10.1002/eqe.395

PEER (Pacific Earthquake Engineering Research Centre) (2013). http://peer.berkeley.edu/smcat/data. Accessed 15 Dec 2014

Phan V, Saiidi MS, Anderson J, Ghasemi H (2007) Near-fault ground motion effects on reinforced concrete bridge columns. J Struct Eng 133(7):982–989. https://doi.org/10.1061/(ASCE)0733-9445

Providakis CP (2007) Pushover analysis of base isolated steel concrete composite structures under near fault excitations. Soil Dyn Earthq Eng 28:293–304. https://doi.org/10.1016/j.soildyn.2007.06.012

Shen J, Tsai M, Chang K, Lee GC (2004) Performance of a seismically isolated bridge under near-fault earthquake ground motions. J Struct Eng 130(6):861–868. https://doi.org/10.1061/(ASCE)0733-9445

Stamatopoulos GN (2012) Response of a wind turbine subjected to near-fault excitation and comparison with the Greek Aseismic Code provisions. Soil Dyn Earthq Eng 46:77–84. https://doi.org/10.1016/j.soildyn.2012.12.014

Su C, Sung Y, Chang S, Huang C (2007) Analytical investigations of seismic responses for reinforced concrete bridge columns subjected to strong near-fault ground motion. Earthq Eng Eng Vib 6(3):237–244. https://doi.org/10.1007/s11803-007-0757-8

Tzimas AS, Kamaris GS, Karavasilis TL, Galasso C (2016) Collapse risk and residual drift performance of steel buildings using post-tensioned MRFs and viscous dampers in near-fault regions. Bull Earthq Eng 14(6):1643–1662. https://doi.org/10.1007/s10518-016-9898-3

Yahyai M, Rezayibana B, Mohammadrezapour E (2011) Effect of near-fault earthquakes with forward directivity on telecommunication towers. Earthq Eng Eng Vib 10(2):211–218. https://doi.org/10.1007/s11803-011-0059-z

Yan X, Lee GC (2007) Traveling wave effect on the seismic response of a steel arch bridge subjected to near fault ground motions. Earthq Eng Eng Vib 6(3):245–257. https://doi.org/10.1007/s11803-007-0761-z

Yazdani Y, Alembagheri M (2017) Effects of base and lift joints on the dynamic response of concrete gravity dams to pulse-like excitations. J Earthq Eng 21(5):840–860. https://doi.org/10.1080/13632469.2016.1185056

Zeinkiewicz OC, Taylor RL (1991) Finite element method. McGraw-Hill, London

Zhang S, Wang G (2013) Effects of near-fault and far-fault ground motions on nonlinear dynamic response and seismic damage of concrete gravity dams. Soil Dyn Earthq Eng 53:217–229. https://doi.org/10.1016/j.soildyn.2013.07.014

Zou D, Han H, Liu J, Yang D, Kong X (2017) Seismic failure analysis for a high concrete face rockfill dam subjected to near-fault pulse-like ground motions. Soil Dyn Earthq Eng 98:235–243. https://doi.org/10.1016/j.soildyn.2017.03.031